AD_____

Award Number: W81XWH-05-1-0291

TITLE: A Partnership Training Program in Breast Cancer Research Using Molecular Imaging Techniques

PRINCIPAL INVESTIGATOR: Paul C. Wang, Ph.D.

CONTRACTING ORGANIZATION: Howard University
Washington, DC 20059

REPORT DATE: July 2007

TYPE OF REPORT: Annual

PREPARED FOR: U.S. Army Medical Research and Materiel Command
Fort Detrick, Maryland 21702-5012

DISTRIBUTION STATEMENT: Approved for Public Release;
Distribution Unlimited

REPORT DOCUMENTATION PAGE

Form Approved
OMB No. 0704-0188

1. REPORT DATE	2. REPORT TYPE	3. DATES COVERED
01-07-2007	Annual	1 Jul 2006 – 30 Jun 2007

4. TITLE AND SUBTITLE

A Partnership Training Program in Breast Cancer Research Using Molecular Imaging Techniques

5a. CONTRACT NUMBER

5b. GRANT NUMBER
W81XWH-05-1-0291

5c. PROGRAM ELEMENT NUMBER

6. AUTHOR(S)

Paul C. Wang, Ph.D.

Email: pwang@howard.edu

5d. PROJECT NUMBER

5e. TASK NUMBER

5f. WORK UNIT NUMBER

7. PERFORMING ORGANIZATION NAME(S) AND ADDRESS(ES)

Howard University
Washington, DC 20059

8. PERFORMING ORGANIZATION REPORT NUMBER

9. SPONSORING / MONITORING AGENCY NAME(S) AND ADDRESS(ES)
U.S. Army Medical Research and Materiel Command
Fort Detrick, Maryland 21702-5012

10. SPONSOR/MONITOR'S ACRONYM(S)

11. SPONSOR/MONITOR'S REPORT NUMBER(S)

12. DISTRIBUTION / AVAILABILITY STATEMENT
Approved for Public Release; Distribution Unlimited

13. SUPPLEMENTARY NOTES

14. ABSTRACT
In the second year, five faculty members and a research assistant were further trained in molecular imaging of breast cancer through seminars and workshops, and are currently conducting two research projects with the faculty at Johns Hopkins University. We have perfected the technique of constructing a dual imaging probe for MRI and fluorescent imaging by linkage of near-infrared fluorescently labeled transferrin on the surface of contrast agent encapsulated cationic liposomes. The dual probe not only enhances the tumor MR image contrast but is also an excellent probe for optical imaging. We have established three breast cancer tumor models including subcutaneous xenografts, mammary gland xenografts, and lung metastasis in nude mice using luciferase-expressing MDA-MB-231-luc cells. Metastatic lesion of 0.3-0.5 mm in diameter could be clearly detected by MRI or optical imaging in vivo. We have found that when MCF-7 cells are co-cultured with activated THP-1 macrophages they caused an increase in PTEN expression. MIF expression is dramatically induced in MCF-7 cells when they are co-cultured with macrophages. We have published three papers and another paper is in press. We have given six presentations in conferences. We received two new grants and five other grant applications are pending. We have recruited a new faulty member to join the project. A research assistant supported by this grant received her undergraduate degree in Biology at the Howard University with summa cum laude. The Molecular Imaging Lab continuously served as a synergic center on campus for promoting molecular imaging research. New research collaborations were established among the faculty at Howard, as well as with the external scientists from Georgetown University and NIH.

15. SUBJECT TERMS
training, molecular imaging, breast cancer, optical imaging, magnetic resonance imaging

16. SECURITY CLASSIFICATION OF:			17. LIMITATION OF ABSTRACT	18. NUMBER OF PAGES	19a. NAME OF RESPONSIBLE PERSON
a. REPORT	b. ABSTRACT	c. THIS PAGE			USAMRMC
U	U	U	UU	55	19b. TELEPHONE NUMBER *(include area code)*

Table of Contents

A Partnership Training Program In Breast Cancer Research Using Molecular Imaging Techniques

I. INTRODUCTION

Advances in molecular and cell biology techniques in recent years have had a marked effect on our understanding of the cellular and molecular mechanisms of cancers, including breast cancer. Significant strides have also been made in the development of a noninvasive, high-resolution, in vivo imaging technology such as positron emission tomography (PET), magnetic resonance imaging (MRI), and optical imaging techniques for better imaging of tumors. In vivo molecular imaging, which utilizes these two fronts, opens up an extraordinary opportunity for studying diseases noninvasively, and in many cases, quantitatively at the molecular level (1-4). Molecular imaging is a growing research discipline aimed at developing and testing novel tools, reagents, and methods to image specific molecular pathways in vivo, particularly those that are key targets in disease processes.

The current assessment of breast cancer depends on anatomic and physiological changes of the disease. These changes are a late manifestation of the molecular changes that truly underlie the disease. If imaging of these early molecular changes is possible, it will directly affect patient care by allowing much earlier detection of the disease. Potentially, clinicians may be able to image molecular changes that currently are defined as "predisease states". This will allow intervention at a time when the outcome is most likely to be affected. In addition, by directly imaging the underlying alterations of disease, the effects of therapy may be monitored shortly after therapy has been initiated in contrast to the many months often required today (5).

In this proposed training program, a partnership between Howard University (HU) and the In Vivo Cellular Molecular Imaging Center (ICMIC) at Johns Hopkins University (JHU) will be established to pursue the molecular imaging research of breast cancer. At Howard University, this partnership will involve a multidisciplinary consortium of five departments. The program is composed of two components: a research component and a broad training component. Howard University faculty will obtain training through conducting collaborative research and by participating in a broad based training program. Experts from Johns Hopkins will participate in training by offering laboratory internships, mentoring research efforts, and conducting seminars and workshops. Through this program, a core facility will also be established to support sustainable long-term molecular imaging research at Howard University.

Our goal for this program is to provide faculty trainees at Howard with basic and updated molecular imaging techniques that they can employ while conducting breast cancer research. The program objectives are:

1. Train new researchers in the breast cancer imaging field using molecular imaging techniques.
2. Offer molecular imaging and breast cancer-related lectures, seminars, workshops, and laboratory internships.
3. Conduct two proposed research projects:
    a. Magnetic Resonance (MR) Image Enhancement by Tumor Cell Targeted Immunoliposome Complex Delivered Contrast Agent.
    b. Imaging the Effects of Macrophage Function on Tumor Progression.
4. Establish a molecular imaging core to support long-term sustainable research.
5. Research concept development and submission grants in breast cancer imaging.

II. BODY

This training program consists of two components: a research component and a broad based training component. The research component includes two research projects and the establishment of a molecular imaging core facility at Howard University. A general description and the progress of the each component are listed as follows:

II.1 Research Components: (a) Research Projects (b) Establish a Molecular Imaging Core Facility

(a) Research Projects:

Project 1: MR Image Enhancement by Tumor Cell Targeted Immunoliposome Complex Delivered Contrast Agent

Tumor imaging exploits the differences in physical properties between malignant and normal tissues. These differences are often insufficient for good contrast resolution (5). Imaging techniques that improve tumor detection, localization and evaluation of therapy and prognosis would be highly desirable (6, 7). Contrast-enhanced magnetic resonance imaging is one of the best noninvasive methodologies available today in clinical medicine for assessing anatomy and function of tissues (8). High spatial resolution and high soft tissue contrast are desirable features of noninvasive MRI. However, due to intrinsically low sensitivity, high local concentration of contrast agents (CA) is required to generate detectable MR contrast. A large amount of CA has to be used due to the non-specific uptake by tumors and other tissues *in vivo*. In recent years, targeted CA delivery systems have been developing based on the concept that molecular imaging can increase the signal to noise ratio by detecting the difference in 'molecular properties' between cancer and normal tissues (9-11). This should, in theory, allow for detection of smaller tumors. As one strategy, monoclonal antibodies or antibody fragments have been coupled with CA directly or linked with CA through liposome (Lip) carrier. High concentration of antibody-mediated CA such as Gd provides high T1 positive contrast *in vivo*, but insufficient direct linkage of Gd with antibody or the large molecular size of antibody-Lip-Gd particles may limit its use for imaging cell-surface receptors in solid tumors because of inefficient extravasation and very slow diffusion in the interstitial compartment (6, 12, 13). Furthermore, antibody immunogenicity, poor stability of the conjugates and potential change of the antibody binding ability due to changes in surface antigens are still problematic for *in vivo* application. A ligand with less toxic, high binding specificity for tumors, relative small size and without immunogenicity is required to target the CA to tumors.

Optical imaging offers several advantages over other imaging techniques. Among these are simplicity of the technique, high sensitivity and absence of ionizing radiation. There is a general increase in the development of techniques for *in vivo* evaluation of gene expression, monitoring of gene delivery and real-time intraoperative visualization of tumor margins and metastatic lesions to improve surgical outcome (14-16). Limited depth of light penetration and lack of tomographic information prevent *in vivo* efficiency of optical imaging. In order to overcome the limitations of various imaging modalities, multimodal probes have been developed for detection using multiple imaging devices (17-19).

Transferrin receptor (TfR) is a cell-surface internalizing receptor responsible for almost all iron sequestration in mammalian cells. Overexpression of TfR is reported on human cancers from various tissues including breast and is of great value in grading tumors and determining

prognosis (20). TfR has been successfully applied as a molecular target to direct therapeutic agents to tumor cells (21). Transferrin (Tf), the TfR ligand, is a monomeric glycoprotein that binds Fe^{3+} atoms for delivery to vertebrate cells through receptor-mediated endocytosis. Fluorescently labeled Tf has greatly aided the investigation of endocytosis *in vitro*. *In vivo* use of the physiological serum protein Tf is less likely to cause adverse reactions. Indeed, Tf has been successfully used in targeted gene therapy (22,23). We hypothesized that near-infrared dye (NIR) labeled Tf (Tf^{NIR}) would be an ideal ligand and would selectively increase the cellular uptake of MRI and optical reporters *in vivo*, resulting in contrast-enhanced MRI and NIR-based optical detection. Herein, we developed a Tf- and Lip-mediated dual molecular probe with both fluorescent and magnetic reporter groups. The Tf^{NIR} was linked on the surface of Lip, whereas the MRI CA (Magnevist) was encapsulated within the Lip. These components conjugated together and formed uniform vesicles with less than 100 nm in diameter. *In vitro* analysis demonstrated that the probe dramatically improved the uptake of CA and NIR dye in culture cells through both receptor- and Lip-mediated endocytosis. *In vivo*, the probe significantly enhanced the magnetic resonance signals from the tumors and was superior to the CA alone for identifying the tumor morphology and infrastructure. Simultaneously a significant preferential accumulation of fluorescent signal by the tumors was clearly detectable in Tf^{NIR}-based optical imaging. Based on these findings, we have published a paper on the J Molecular Imaging (listed in the Reportable Outcomes) and a second manuscript entitled "Dual Probe with Fluorescent and Magnetic Properties for Imaging Solid Tumor Xenografts" (listed in the Appendices) has been submitted for publication.

Project 2: Imaging the Effects of Macrophage Function on Tumor Promotion

We have analyzed MCF-7 breast cancer cells and THP-1-derived macrophages with respect to survival signaling, prior to co-culture with activated macrophages. Recent studies have implicated the inflammatory cytokine macrophage migration inhibitory factor (MIF) in tumor progression, in a variety of cancers, including breast cancer. A striking property of secreted MIF is its ability to inhibit p53. We have examined the expression of the *p53* and *PTEN* tumor suppressor genes, and the effect of recombinant human MIF on the expression of these genes in breast cancer cells and macrophages. While the role of p53 in inducing cell cycle arrest and apoptosis is well established, it has recently been shown that these two tumor suppressors function collaboratively in a tumor-suppressive network: p53 transactivates the *PTEN* gene and PTEN protein spares p53 from proteasomal degradation by inhibiting the PI3K-AKT pathway. AKT phosphorylation of MDM2 facilitates MDM2 entry into the nucleus, where it binds p53 and transports it out of the nucleus for proteasomal degradation. MDM2-mediated loss of p53 function promotes tumor cell survival and resistance to chemotherapy. PTEN suppresses the PI3K-AKT pathway, a major survival signaling pathway, thereby sparing p53 from degradation. PTEN physically binds p53 protein resulting in stabilization of p53, which up-regulates *PTEN* expression. However, an increase in p53 protein levels results in a decrease of PTEN stability, an apparent counter-regulatory mechanism that maintains a balance between these two tumor suppressors and prevents an exaggerated apoptotic response. It is, therefore, important to know the *p53* and *PTEN* expression status of MCF-7 cells both before and after co-culture with THP-1-derived macrophages.

Our results show that MCF-10A (immortalized mammary epithelial) cells have the highest levels of PTEN mRNA, consistent with their being non-tumorigenic. Co-culture of MCF-7 with activated THP-1 macrophages caused an increase in *PTEN* expression (Fig. 1).

Recombinant human MIF (rhMIF) suppressed *p53* expression in all cell types (Fig. 2). Suppression of p53 in MCF-7 would inhibit apoptosis, promote survival, and increase drug resistance. MIF is secreted by both cancer cells and tumor-assoicated macrophages (TAMs). MIF-mediated loss of p53 function, without p53 mutation, would allow cancer cells to accumulate oncogenic mutations that produce a more aggressive phenotype, in the absence of any selective pressure for loss of p53 in either epithelial or stromal cells. MIF expression is dramatically induced in MCF-7 cells when they are co-cultured with macrophages (Fig. 3).

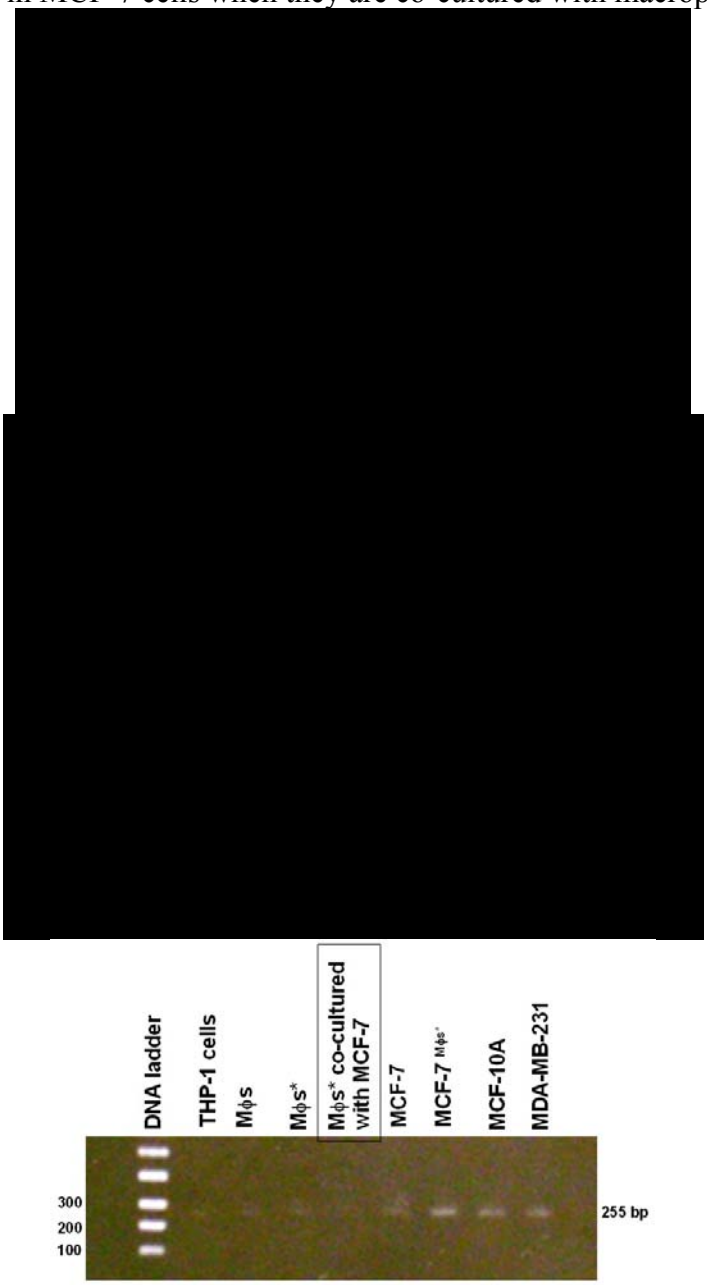

Fig. 3. RT-PCR of MIF mRNA in breast cancer cells and macrophages. All cells studied readily expressed MIF mRNA. In Mϕs* co-cultured with MCF-7, *MIF* RNA expression was downregulated when compared with Mϕs*

(b) Establish a Molecular Imaging Core Facility

It is essential for Howard to establish a basic infrastructure that is capable of supporting a sustainable long-term research program in the field of molecular imaging of breast cancer after this training program. This infrastructure is necessary to provide the researchers with tools to perform the proposed researched projects as well as to provide a broader research training experience. The core of the infrastructure is built upon the existing Biomedical NMR Laboratory in the Howard University Cancer Center. The Biomedical NMR Laboratory has two NMR machines capable of small animal imaging. Through this program, we have acquired a fluorescent and luminescence imaging instrument (Xenogen IVIS 200), which enables us to study stromal inflammation and the internalization of contrast agent in tumor. This new optical imaging instrument has significantly enhanced the molecular imaging capabilities of the research core at Howard University. This has complemented the existing NMR imaging facility at Howard University. The core facility also includes other optical instruments such as a fluorescent microscope. The staff of the molecular imaging core includes an imaging scientist, a molecular biologist, a chemist, a research assistant, and the staff from the Biomedical NMR Laboratory. An important mission of the Molecular Imaging Core Facility is to attract more faculty members into molecular imaging research and serve as a center to train future minority scientists in this field.

II.2 Broad Based Training Components

The Molecular Imaging Lab has regular bi-weekly group meetings, journal club, and seminars. The faculty trainees have also attended four special workshops on molecular imaging and imaging instrumentation. There were four special guest seminars on molecular imaging. The trainees have also attended various seminars at JHU ICMIC. The trainees have an in-depth group meeting with faculty from JHU to exchange ideas and discussing various aspects of the research. The PI and the partnership leader at JHU have been coordinating the training efforts through meetings and emails.

II.2.a. Seminars at Howard University

1. *In vivo* cancer targeting and imaging with semiconductor quantum dots**.** Dr. Dnyanesh N. Tipre, Wednesday, Sept. 6, 2006
2. Synthesis, Surface and Colloidal Chemistry Studies of Nanocrystalline Magnetic Materials. Dr. Vladimir Kolesnichenko, Xavier University of Louisiana, 10/06/2006
3. Visualization of tumors and metastases in live animals with bacteria and vaccinia virus encoding light-emitting proteins. Dr. Liang Shan, Friday, 10/13/06
4. Mucin expression in cancer and design of mucin peptides for imaging. Dr. Xiaowu Pang, 11/22/2006
5. An introduction to diffusion tensor magnetic resonance imaging and its application. Dr. Alexandru Korotcov,Tuesday, 11/28/2006
6. Chemotherapeutic Platinum Compound Transport and Resistance in Tumorr. Xing Jie Liang, National Institute of Neurological Disorder and Stroke, NIH, 1/30/2007.
7. Construction, Recognition, and Imaging of Novel Tumor-Targeted Agents. Dr. Yunpeng Ye, Washington University School of Medicine, 2/6/2007

8. Mass Spectrometry at the Chemistry/Biology Interface; and Natural Products as Precursors for Industrial Materials. Dr. Folahan O. Ayorinde, Department of Chemistry, Howard University, 02/14/2007
9. Bio-Inspired Materials: Synthesis and Modification of Functional Polymers and Application to Biomineralization. Dr. Tongxin Wang, University of Pennsylvania, 3/1/07

II.2.b. Seminars at Johns Hopkins University

1. Combined anti-angiogenic therapy and siRNA targeting of Choline kinase. Dr. Zaver Bhujwalla, JHU, 6/28/06
2. Optical imaging of lysosomes in breast cancer cells and tumors. Dr. Kristine Glunde, JHU, 9/20/06
3. Molecular imaging of cells and tissue with a mass spectrometer. Dr.Ron Heenen, Utrecht University, Netherlands, 11/20/06
4. Comprehensive review of JHU ICMIC program. Dr. Zaver Bhujwalla, JHU, 12/13/06
5. Multi-modality imaging. Dr. Ronald Basberg, Memorial Sloan-Kettering Cancer Center, 3/21/07
6. Liposome-based systems for in vivo and in vitro delivery of functional and analytical agents. In vitro studies on the control of lymphatic cell motility. Dr. Maria Mikhaylova, JHU, 4/4/07
7. Role of the tumor Microenvironment in prostate cancer xenograft metastasis. Dr. Marie-France Penet, JHU, 4/25/07

II.2.c. Workshops and Training Courses

1. Workshop on Atomic Spectroscopy. PerkinElmer, September 12, 2006, Greenbelt, MD.
2. Introduction to ParaVision. Bruker Biospin MRI, Inc. 09/11-15/2006, Billerica MA.
3. Small Animal Imaging Hands-On Workshop, Johns Hopkins University, February 7-8, 2007.
4. Nanomaterials in Biology and Medicine: Promises and Perils. Arthur M. Sackler Colloquia, National Academy of Sciences, April 10-11, 2007, Washington, D.C.

II.3 Statement of Work

(The bold typed accomplishments are occurred in this reporting period).

Task 1. To conduct the study "MR Image Enhancement by Tumor Cell Targeted mmunoliposome Complex Delivered Contrast Agent"

a. Purchase supplies for cell culture and materials for construction of liposome (Months 1-2) (completed)
b. Construct and measure the size of liposome (Months 3-4) (completed)
c. Attach ligands (single chain variable fragment of transferring antibody) to liposome (TfR-scFv-Lip) (Months 5-8) (completed).
d. Make TfR-scFv-Lip-contrast agent complex. Measure the size of complex and amount of contrast agent encapsulated in the liposome (Month 9-12) (completed).
e. In vitro imaging of transfected MDA-MB-231 breast cancer cells in pellet (Month 13-24) (**completed**)
f. Verify the transfection efficiency by MRI and optical imaging (Month 19-24)

(**completed)**

g. Animal Study: Grow tumor xenografts on nude mice. In vivo MRI imaging of 120 tumor-bearing mice administered TfR-scFv-Lip-CA, Lip-CA, and CA only, using T1 and T2 weighted MRI imaging techniques (Months 27-45) (**in progress)**
h. Quantify the contrast enhancement. Image data analysis (Months 27-45).

Task 2. To conduct the study "Imaging the Effects of Macrophage Function on Tumor Promotion"

- Determine the effects of macrophages on metastasis-related gene expression in breast cancer cells (Months 1 – 24) (**in progress)**.
  a. Measure migratory and invasive properties of breast cell lines that are co-cultured with macrophages: changes in anchorage-dependent cell growth, invasion through matrigel (Months 1 – 12) **(in progress).**
  b. Isolate RNA for gene expression analysis using gene arrays. Monitor expression of proinvasive integrins, MMPs, and TIMPs, etc. (Months 6 – 18) **(in progress)**.
  c. Transfect MCF-12A (mammary epithelial cells), MDA-MB-231, and MDA-MB-468 cancer cells with luciferase construct. Screen luciferase-expressing cells and isolate stable clones by limiting dilution (Months 8 – 24) **(in progress)**.
- Determine the effects of co-culture with macrophages on the growth of Luc^+ mammary epithelial cells and breast cancer cells in 20 athymic nu/nu mice (Months 24 – 48).
  a. Luc^+ MCF-7 cells (in development) and MDA-MB-231 cells will be obtained from Xenogen. Luc^+ mammary epithelial and breast cancer cells co-cultured with macrophages (LPS activated or unactivated). Inject breast cells into athymic mice and monitor with the Xenogen IVIS™ Imaging System. (Month 24-48). **(in progress)**
  b. Repeat gene expression experiments in Luc^+ cells to correlate gene expression patterns with *in vivo* growth (Months 36 – 48).

Task 3. To establish a molecular imaging core facility.

a. Purchase laboratory supplies (months 1-4) (completed).
b. Purchase Xenogen IVIS imaging system (months 3-9) (completed).
c. Establish the designated Molecular Imaging Core Facility in Cancer Center (Rm B103). Install incubator and hood. (Months 3-9) (completed).
d. Relocate/centralize all the molecular biology instruments to the Molecular Imaging Core Facility (Months 3-9) (completed).
e. Training on Xenogen IVIS imaging system (Month 10) (completed).
f. Molecular Imaging Core Facility open house (Month 10) (completed).

Task 4. To train faculty trainees in molecular imaging research.

a. Biweekly group meetings (organized by research leaders) (Months 1-48) (**in progress)**.
b. Monthly journal clubs (Months 1-48) (**in progress)**.
c. Seminar series (nine seminars each year) (Months 1-48) (**in progress)**.
d. Six workshops (chaired by Dr. Wang and Dr. Bhujwalla) (months 1-18) (**in progress)**.
e. Laboratory Internships (2 days to one week each) (Months 1-18) (**in progress)**.
f. Research concepts development (Months 24-36).
g. Research grants submission (Months 37-48).

*Task 5. Administrative and communication affairs (coordinated by Dr. Wang and Dr. Bhujwalla). (Months 1-48) (***in progress***).*

a. Status reports (monthly, quarterly, and annual reports).
b. Research progress review (quarterly).
c. Administrative meetings (biannually meetings).
d. Coordination of seminars, workshops, and laboratory internships.

III. KEY RESEARCH ACCOMPLISHEMENTS

Project 1: MR Image Enhancement by Tumor Cell Targeted Immunoliposome Complex Delivered Contrast Agent

- We have perfected the technique of constructing a dual imaging probe for MRI and fluorescent imaging by linkage of near-infrared (NIR) fluorescently labeled transferrin (TfNIR) on the surface of contrast agent (CA)-encapsulated cationic liposomes (TfNIR-LipNBD-CA).
- The size of the nano-sized dual probe is controlled by gel filtration and its size (~80 nm) was determined by laser light scattering technique. The amount of MR contrast agent encapsulated in the liposome was measured by the atomic absorption spectroscopy.
- Using confocal microscopy, fluorescent imaging, and MRI, we have confirmed that the cellular uptake of both fluorescent and magnetic reporter groups was significantly increased compared to that of fluorescent dye or MR contrast agent alone.
- The dual probe not only enhances the tumor MR image contrast but also is an excellent probe for NIR optical imaging. The probe is also superior to the MR contrast agent for identifying the tumor pathology.
- Three human breast cancer models including subcutaneous tumor xenografts, mammary gland xenografts and lung metastasis in nude mice were also established using luciferase-expressing MDA-MB-231-luc cells. The MDA-MB-231-luc cell line has been transfected with the luciferase gene for bioluminescent optical imaging.
- Dynamic optical imaging of MDA-MB-231-luc tumors growing on the mouse back or on the mammary gland fat pad showed the luminescent image intensity increased to its peak in ~ 20 minutes and gradually diminished about one hour after intraperitoneal injection of D-luciferin.
- A significant correlation between tumor volume and optical signal intensity of luminescent images in tumor was established. Metastatic lesion of 0.3-0.5 mm in d iameter could be clearly detected in vivo.

Project 2: Imaging the Effects of Macrophages on Breast Cancer Metastasis

- MCF-10A (immortalized mammary epithelial) cells have the highest levels of phosphatase and tensin homology gene PTEN mRNA compared with MCF-7 and MDA-MB-231, which is consistent with their being non-tumorigenic.
- Co-culture of MCF-7 with activated human monocytic leukemia, THP-1, derived macrophages caused an increase in PTEN expression.
- Migration inhibitory factor (MIF) expression is dramatically induced in MCF-7 cells when they are co-cultured with macrophages.

IV. REPORTABLE OUTCOMES

Research

Publications (Reprints listed in the appendices section)

1. Shan L, Wang S, Sridhar R, Bhujwalla ZM, Wang PC. Dual Probe with Fluorescent and Magnetic Properties for Imaging Solid Tumor Xenografts. Mol Imaging 6:85-95, 2007
2. Shan L, Wang SP, Zhou YF, Korotcov A, Sridhar R, Wang PC. Optical imaging of transferrin receptors: Dynamic difference in tumor xenografts. Ethnicity and Disease. 2007 (in press).
3. Ross, S, Ejofodomi O, Zheng J, Lo B, Chouikha M, Jendoubi A, Wang P. A Mammography Database and View System for the African American Patients. J Digit Imaging Mar 29 (online first), 2007
4. Bratasz A, Weir NM, Parinandi NL, Zweier JL, Sridhar R, Ignarro LJ, Kuppusamy P. Reversal to Cisplatin Sensitivity in Recurrent Human Ovarian Cancer Cells by NCX-4016, a Nitro Derivative of Aspirin. PNAS 103:3914-3919, 2006

Presentations

1. Wang PC, Shan L, Wang SP, Sridhar R, Bhujwalla ZM. A Dual Probe with Both Fluorescent and MR Reporters for Imaging Solid Tumor Xenografts. The Fifth Annual Meeting of the Society of Molecular Imaging. Big Island, Hawaii, August 30 – September 2, 2006.
2. Wang PC. Molecular Imaging of Solid Tumor Xenografts Using a Dual Fluorescent and MR Probe. College of Pharmacy, Howard University, September 22, 2006.
3. Shan L, Wang SP, Zhou YF, Wang PC. In Vivo Optical Imaging of Transferrin Receptors: Visualization of Tumor Biomarkers. The 5th Asian-Pacific Organization for Cell Biology Congress. Beijing, China, October 28-30, 2006.
4. Wang PC, Shan L, Wang SP, Sridhar R, Bhujwalla ZM. Molecular Imaging of Solid Tumor Xenografts Using a Dual Fluorescent and MR Probe. 10th RCMI International Symposium on AIDS and Health Disparities. San Juan, Puerto Rico, December 13-16, 2006.
5. Renshu Zhang, Liang Shan, Yanfei Zhou, Paul C. Wang, Rajagopalan Sridhar. Rapid detection of cell death in a bioluminescent human breast cancer cell line subjected to hyperthermia. AACR annual meeting, April 14-18, 2007, Los Angels, CA
6. Chung DW, Tsai YS, Miaou SG, Chang WH, Chang YJ, Chen SC, Hong YY, Chyang CS, Chang QS, Hsu HY, Hsu J, Yao WC, Hsu MS, Hsu C, Maio L, Byrd K, Chouikha MF, Gu XB, Wang PC, Szu H. Saliva Portable Kit Reducing Diabetes Un-wanted Blood Tests. Defense & Security Sym.: ICA Wavelets Unsupervised Learning Nano-Biomimetic Sensors Neural Net Conf., SPIE Proc V. 6576 (Szu ed.) April 9-13, 2007, Orlando FL.

Degree Obtained

1. Giselle Burnett, a research assistant supported by this grant in the summer 2006, received B.S. degree in Biology at Howard University, in June, 2007. She has been accepted by the Howard University Medical School. However, she has decided to defer the enrollment until 2008. She will continue working with Dr. Bremner on the Project 2

"Imaging the Effects of Macrophage Function on Tumor Promotion". She will be supported by this grant as a research assistant in the year 2007-08.

Grants

Received

1. Tumor-targeted MR contrast enhancement using molecular imaging TechniquesNIH, 5U54 CA091431-06A1, 09/06-08/09, Paul C Wang (PI), Zaver M Bhujwalla (co-PI)
2. Targeted Fluorescent Microspheres for Noninvasive Optical Detection of Tumors, Charles & Mary Latham Fund, 01/01/07-12/31/07, Liang Shan (PI)

Submitted Pending Grants

1. Salvia miltiorrhiza Bge as a new chemopreventive agent for oral cancer, NIH, resubmission, 11/16/2006
2. Xinbin Gu (PI), Hongguang Ji, Xiaowu Pang, Rajagopalan Sridhar, Tianpei Xie, Joseph Califano, Esther Childers, Paul Wang
3. Investigation of salvianolic acid B nanoparticles in oral cancer, Mordecai Wyatt Johnson Award resubmission, Xinbin Gu (PI), Eric Walter, Paul Wang
4. Enhance necrosis and sensitize chemotherapy in prostate cancer by inhibition of histone deacetylase SIRT1, Army Prostate Cancer Program, submitted 5/11/2007, Xing-Jie Liang (PI)
5. Visualizing interactions of human glioblastoma stem cells with tumor infiltrating lymphocytes through brain imaging, Dana Program in Brain and Immuno-imaging, submitted 5/21/2007, Xing-Jie Liang (PI)

Unfunded Grant Submissions

1. Novel Targeted Gd-Nanosphere MRI Contrast Agent For Breast Cancer Imaging, DoD Breast Cancer Synergistic Idea Award, Liang Shan, Paul C Wang, Chuck Zhang
2. Affordable and Accessible Point-of-Care for Howard University Hospital Community Geriatrics NIH, Paul C Wang (PI), Xinbin Gu, Xiaowu Pang, Alexandru Korotcov, Wayne Frederick, Lucile Adams-Campbell, Mohamed Chouikha.

Employment

1. Dr. James Mack, who was a faculty trainee, has left the university and went to join NIH Center for Scientific Review, Biological Chemistry and Macromolecular Biophysics Integrated Review as a administrator.
2. Dr. Xing-Jie Liang, an assistant professor in the Department of Radiology, is a new faculty trainee replacing Dr. Mack. Dr. Liang will start on July 1, 2007. Dr. Liang was a research fellow at NIH/NCI with Dr. Michael Gottesman. His expertise is in the cellular and molecular mechanism of drug resistance of chemotherapy. He will work on developing nano particles specifically targeting cancer cells for drug delivery. His CV is attached in the appendix.

V. CONCLUSIONS

In the second year, this training grant continuously progressed well. Five faculty members and a research assistant from Departments of Biology, Radiology, and Radiation

Oncology at Howard University were further trained in molecular imaging through seminars and workshops, and are conducting two research projects with the faculty at the In Vivo Cellular Molecular Imaging Center at the Johns Hopkins University.

We have perfected the technique of constructing a dual imaging probe for MRI and fluorescent imaging by linkage of near-infrared fluorescently labeled transferrin on the surface of contrast agent encapsulated cationic liposomes. The dual probe not only enhances the tumor MR image contrast but is also an excellent probe for NIR optical imaging. The probe is also superior to the MR contrast agent for identifying the tumor pathology. We have established three breast cancer tumor models including subcutaneous xenografts, mammary gland xenografts, and lung metastasis in nude mice using luciferase-expressing MDA-MB-231-luc cells. Dynamic optical imaging of MDA-MB-231-luc tumors showed the luminescent image intensity increased to its peak in ~ 20 minutes and gradually diminished after about one hour. A significant correlation between tumor volume and optical signal intensity of luminescent images in tumor was established. Metastatic lesion of 0.3-0.5 mm in diameter could be clearly detected in vivo.

We have shown that non-tumorigenic mammary epithelial MCF-10A cells have the highest levels of PTEN mRNA compared with MCF7 and MDA-MB-231 cells. When MCF-7 co-cultured with activated THP-1 macrophages caused an increase in PTEN expression. We also found that recombinant human migration inhibitory factor suppressed *p53* expression in all three cell types tested. MIF expression is dramatically induced in MCF-7 cells when they are co-cultured with macrophages.

In this year we have published three papers and another paper is in press. We have given six presentations in the conferences. We received two new grants and five other grant applications are pending. We have recruited a new faulty member to join the project. A research assistant supported by this grant received her undergraduate degree in Biology at the Howard University. The Molecular Imaging Lab continuously served as a synergic center on campus for promoting molecular imaging research. New research collaborations were established among the faculty at Howard, as well as with the external scientists from Georgetown University and NIH.

VI. ABBREVIATIONS

CA	contrast agent
FBS	fetal bovine serum
Gd	gadolinium
hTfR	human transferrin receptor
HU	Howard University
ICMIC	In Vivo Cellular Molecular Imaging Center
JHU	John Hopkins University
Lip	liposome
Luc+	luciferase-positive
MDM2	murine double minute oncogene
MEM	minimum essential medium
MIF	migration inhibitory factor
MR	magnetic resonance
MRI	magnetic resonance imaging
MSR	macrophage scavenger receptor
NIR	near infrared dye
NMR	nuclear magnetic resonance
PBS	phosphate bovine solution
PET	positron emission tomography
PI3K-AKT	phosphatidylinositol-3-kinase and protein kinase B
PTEN	phosphatase and tensin homolog gene
RPMI	medium developed at Rosewell Park Memorial Institute
scFv	single-chain antibody variable fragment
Tf	transferrin
TfNIR	transferrin labeled with near infrared dye
TfR	transferrin receptor
TfR-scFv-Lip	transferrin-single chain variable fragment-liposome
TfR-scFv-Lip-CA	transferrin-single chain variable fragment-liposome-contrast agent
THP-1	human monocytic leukemia cell

VII. REFERENCES

[1] Pautler RG (2004). Mouse MRI: concepts and applications in physiology. *Physiol*. 19:168-175.

[2] Artemov D (2003). Molecular magnetic resonance imaging with targeted contrast agent. *J Cell Biochem*. 90: 518-524.

[3] Massoud TF, Gambhir SS (2003). Molecular imaging in living subjects: seeing fundamental biological processes in a new light. *Gene Dev*. 17:545-580.

[4] Persigehl T, Heindel W, Bremer C (2005). MR and optical approaches to molecular imaging. *Abdom Imaging*. 30:342-354.

[5] Blasberg RG (2003). Molecular imaging and cancer. *Mol Cancer Ther*. 2:335-345.

[6] Funovics MA, Kapeller B, Hoeller C, Su HS, Kunstfeld R, Puig S, Macfelda K (2004). MR imaging of the her2/neu and 9.2.27 tumor antigens using immunospecific contrast agents. *Magn Reson Imaging*. 22:843-850.

[7] Basilion JP (2001). Current and future technologies for breast cancer imaging. *Breast Cancer Res*. 3:14-16.

[8] Artemov D, Mori N, Okollie B, Bhujwalla ZM (2003). MR molecular imaging of HER-2/neu receptor in breast cancer cells using targeted iron oxide nanoparticles, *Magn Reson Med*. 49:403-408.

[9] Mulder WJM, Strijkers GJ, Griffioen AW, van Bloois L, Molema G, Storm G, Koning GA, Nicolay K (2004). A liposomal system for contrast-enhanced magnetic resonance imaging of molecular targets. *Bioconjugate Chem*. 15:799-806.

[10] Jones DT, Trowbridge IS, Harris AL (2006). Effects of transferrin receptor blockade on cancer cell proliferation and hypoxia-inducible factor function and their differential regulation by ascorbate. *Cancer Res*. 66:2749-2756.

[11] Hogemann-Savellano D, Bos E, Blondet C, Sato F, Abe T, Josephson L, Weissleder R, Gaudet J, Sgroi D, Peters PJ, Basilion JP (2003). The transferrin receptor: a potential molecular imaging marker for human cancer. *Neoplasia*. 5:495-506.

[12] Batra JK, Fitzgerald DJ, Chaudhary VK, Pastan I (1991). Single-chain immunotoxins directed at the human transferrin receptor containing Pseudomonasexotoxin A or diphtheria toxin: Anti-TFR(Fv)-PE40 and DT388-anti-TFR(Fv). MolCellBiol.11:2200–2205.

[13] Jain RK, Baxter LT (1988). Mechanisms of heterogenous distribution of monoclonal antibodies and other macro-molecules in tumors: Significance of elevated interstitial pressure. CancerRes.48:7022–7032.

[14] Xu L, Tang WH, Huang CC, Alexander W, Xiang LM, Pirollo KF, Rait A, Chang EH (2001). Systemic p53 gene therapy of cancer with immunolipoplexes targeted by anti-transferrin receptor scFv. MolMed.7:723–734.

[15] Xu L, Huang C-C, Huang W-Q, Tang W-H, Rait A, Yin Y, Cruz I, Xiang L-M, Pirollo K, Chang EH (2002). Systemic tumor-targeted gene delivery by anti-transferrin receptor scFv-immunolipo-somes. MolCancerTher.1:337–346.

[16] Xu L, Pirollo KF, Tang Wh, Rait A, Chang EH (1999). Transferrin-liposome-mediated systemic p53 gene therapy in combination with radiation results in regression of human head and neck cancer xenographs. *Hum Gene Ther*. 10:2941-2952.

[17] Bellocq NC, Pun SH, Jensen GS, Davis ME (2003). Transferrin-containing, cyclodextrin polymer-based particles for tumor-targeted gene delivery. *Bioconjugate Chem*. 14:1122-1132.

VIII. APPENDICES

1. Shan L, Wang S, Sridhar R, Bhujwalla ZM, Wang PC. Dual Probe with Fluorescent and Magnetic Properties for Imaging Solid Tumor Xenografts. Mol Imaging 6:85-95, 2007
2. Shan L, Wang SP, Zhou YF, Korotcov A, Sridhar R, Wang PC. Optical imaging of transferrin receptors: Dynamic difference in tumor xenografts. Ethnicity and Disease. 2007 (in press).
3. Ross, S, Ejofodomi O, Zheng J, Lo B, Chouikha M, Jendoubi A, Wang P. A Mammography Database and View System for the African American Patients. J Digit Imaging Mar 29 (online first), 2007
4. Bratasz A, Weir NM, Parinandi NL, Zweier JL, Sridhar R, Ignarro LJ, Kuppusamy P. Reversal to Cisplatin Sensitivity in Recurrent Human Ovarian Cancer Cells by NCX-4016, a Nitro Derivative of Aspirin. PNAS 103:3914-3919, 2006
5. Dr. Xing-Jie Liang's curriculum vitae.

Dual Probe with Fluorescent and Magnetic Properties for Imaging Solid Tumor Xenografts

Liang Shan, Songping Wang, Rajagopalan Sridhar, Zaver M. Bhujwalla, and Paul C. Wang

Abstract

A dual probe with fluorescent and magnetic reporter groups was constructed by linkage of the near-infrared (NIR) fluorescent transferrin conjugate (Tf^{NIR}) on the surface of contrast agent–encapsulated cationic liposome (Lip-CA). This probe was used for magnetic resonance imaging (MRI) and optical imaging of MDA-MB-231-luc breast cancer cells grown as a monolayer in vitro and as solid tumor xenografts in nude mice. Confocal microscopy, optical imaging, and MRI showed a dramatic increase of in vitro cellular uptake of the fluorescent and magnetic reporter groups from the probe compared with the uptake of contrast agent or Lip-CA alone. Pretreatment with transferrin (Tf) blocked uptake of the probe reporters, indicating the importance and specificity of the Tf moiety for targeting. Intravenous administration of the dual probe to nude mice significantly enhanced the tumor contrast in MRI, and preferential accumulation of the fluorescent signal was clearly seen in NIR-based optical images. More interestingly, the contrast enhancement in MRI showed a heterogeneous pattern within tumors, which reflected the tumor's morphologic heterogeneity. These results indicate that the newly developed dual probe enhances the tumor image contrast and is superior to contrast agent alone for identifying the tumor pathologic features on the basis of MRI but also is suitable for NIR-based optical imaging.

TUMOR IMAGING exploits the differences in physical properties between malignant and normal tissues. These differences are often insufficient for good contrast resolution.[1–3] Contrast-enhanced magnetic resonance imaging (MRI) is one of the best noninvasive methodologies available today in clinical medicine for assessing the anatomy and function of tissues.[4] High spatial resolution and high soft tissue contrast are desirable features of noninvasive MRI. However, owing to intrinsically low sensitivity, high local concentration of contrast agents (CAs) is required to generate detectable magnetic resonance contrast. A large amount of CA has to be used owing to the nonspecific uptake by tumors and other tissues in vivo. In recent years, targeted CA delivery systems have been developing based on the concept that molecular imaging can increase the signal to noise ratio by detecting differences in 'molecular properties' between cancer and normal tissues.[5–7] This should, in theory, allow for detection of smaller tumors. As one strategy, monoclonal antibodies or antibody fragments have been coupled with CA directly or linked with CA through liposome (Lip) carrier. However, insufficient direct linkage of gadolinium (Gd) with antibody or the relatively large molecular size of antibody-Lip-Gd particles may limit its use as a CA for imaging cell surface receptors in solid tumors because of inefficient extravasation and very slow diffusion in the interstitial compartment.[2,8,9] Furthermore, antibody immunogenicity, poor stability of the conjugates, and potential change of the antibody binding ability owing to changes in surface antigens are still problematic for in vivo application. A ligand with less toxic, high binding specificity for tumors and relatively small size and without immunogenicity is required to target the CA to tumors.

Optical imaging offers several advantages over other imaging techniques. Among these are the simplicity of the technique, high sensitivity, and absence of ionizing radiation. There is increasing interest in the development of techniques for in vivo evaluation of gene expression, monitoring of gene delivery, and real-time intraoperative

From the Departments of Radiology and Radiation Oncology, Howard University, Washington, DC; and Department of Radiology, Johns Hopkins University School of Medicine, Baltimore, MD.

This study was made possible by grant number 2G12RR003048 from the National Center for Research Resources, a component of the National Institutes of Health (NIH). It was also supported by the following grants: USAMRMC W81XWH-05-1-0291, DAMD17-00-1-0291, DAMD17-03-1-0759, and NIH 5U54CA091431.

Address reprint requests to: Paul C. Wang, PhD, Department of Radiology, Howard University, 2041 Georgia Avenue, NW, Washington, DC 20060; e-mail: pwang@howard.edu.

DOI 10.2310/7290.2007.00006

visualization of tumor margins and metastatic lesions to improve surgical outcome.[10–12] Limited depth of light penetration and a lack of tomographic information prevent in vivo efficiency of optical imaging. To overcome the limitations of various imaging modalities, multimodal probes have been developed for detection using multiple imaging devices.[13–15]

Transferrin receptor (TfR) is a cell surface internalizing receptor that is responsible for almost all iron sequestration in mammalian cells. TfR is overexpressed in 74% of breast carcinomas, 76% of lung adenocarcinomas, and 93% of lung squamous cell carcinomas. The expression level of TfR receptor is of great value in grading tumors and determining prognosis.[16,17] TfR has been successfully applied as a molecular target to direct therapeutic agents to tumor cells.[17] Transferrin (Tf), the TfR ligand, is a monomeric glycoprotein that binds Fe^{3+} for delivery to vertebrate cells through receptor-mediated endocytosis. Fluorescently labeled Tf has greatly aided the investigation of endocytosis in vitro. Tf has also been successfully used in targeted gene therapy in vivo.[18,19] We hypothesized that near-infrared (NIR) dye–labeled Tf (Tf^{NIR}) would be an ideal ligand for targeting MRI and optical reporters to solid tumors, enabling better contrast-enhanced MRI and NIR-based optical detection. We developed a Tf- and Lip-mediated dual molecular probe with both fluorescent and magnetic reporter groups. The Tf^{NIR} was linked on the surface of Lip particles, whereas the MRI CA (Magnevist, obtained from Berlex Laboratories, Wayne, NJ) was encapsulated within the Lip. These components conjugated together and formed small uniform vesicles (less than 100 nm in diameter). In vitro analysis demonstrated that the probe dramatically improved the uptake of CA and NIR dye in monolayer cultures of MDA-MB-231-luc human breast cancer cells through both receptor- and Lip-mediated endocytosis. In vivo, the probe significantly enhanced the magnetic resonance signals from the MDA-MB-231-luc cells grown as solid tumor xenografts in nude mice and was superior to the CA alone for identifying the tumor morphology and infrastructure. Simultaneously, a significant preferential accumulation of fluorescent signal by the tumors was clearly detectable in Tf^{NIR}-based optical imaging.

Materials and Methods

Materials

Cationic lipids including 1,2-dioleoyl-sn-glycero-3-phosphoethanolamine (DOPE), 1,2-dioleoyl-3-trimethylammonium-propane (DOTAP), and fluorescent lipid DOPE-N-(7-nitro-2-1,3-benzoxadiazole-4-yl) (NBD-DOPE) were purchased from Avanti Polar Lipids (Alabaster, AL). They were premixed and dissolved in chloroform in a formula of DOTAP:DOPE (1:1 w/w) (Lip) or in a fluorescent formula of DOTAP:DOPE + 0.1% NBD-DOPE (Lip^{NBD}). Fluorescent Alexa fluor 680 conjugate of human Tf (Tf^{NIR}), a SelectFX nuclear labeling kit, Alexa fluor 680 fluorophore, and enzyme-free phosphate-buffered saline (PBS)-based cell dissociation solution were purchased from Invitrogen (Carlsbad, CA). Holotransferrin without fluorescent conjugate and MicroSpin G-50 columns were obtained from Sigma (St. Louis, MO) and Amersham Biosciences (Piscataway, NJ), respectively. The SPI-Pore polycarbonate membrane filter and filter holder were from Structure Probe Inc (West Chester, PA).

Preparation of the Molecular Dual Probe: Tf^{NIR}-Lip^{NBD}-CA Complex

The Tf^{NIR}-Lip^{NBD}-CA complex was constructed using Tf^{NIR}, cationic Lip^{NBD}, and Magnevist. Premixed Lip^{NBD} in chloroform (3.607 μL) was dried under a nitrogen stream and hydrated by adding 50 μL of water containing 12 μL of Magnevist. Each microliter of Magnevist contains 469.01 μg of gadopentatate dimeglumine. The hydrated Lip^{NBD}-CA mixture was homogenized using a vortex generator and incubated for 10 minutes. The volume of the mixture was adjusted to 175 μL with water. The mixture was then sequentially downsized by sonication (80–90 W, 10 minutes) in a water bath and by repeatedly passing through polycarbonate filters with decreasing pore diameter 0.2/0.1 μm. Following that, 25 μL of Tf^{NIR} (5 mg/mL) was mixed and incubated for at least 10 minutes. Gel filtration through a Sephadex G-50 column was used to remove unencapsulated CA and free Tf^{NIR}. A freshly prepared probe was used in all analysis. The final volume was 200 μL, and Lip:Tf:Magnevist composition was 10:12.5:0.56 (nmol/μg/mg). To monitor different components of the probe, nonfluorescent Tf and Lip were used instead of fluorescent Tf^{NIR} and Lip^{NBD} in some experiments.

Cell Culture and Animal Model

The MDA-MB-231-luc human breast cancer cell line (Xenogen, Alameda, CA) was used to test the efficiency of the probe in vitro and in vivo. This cell line is well documented for constitutional overexpression of TfR and has been transfected with the luciferase gene for luciferase-

based optical imaging. (In this study, we did not use luciferase-based imaging.) Cells were routinely maintained in Dulbecco's Modified Eagle's Medium/F-12 medium supplemented with 10% heat-inactivated fetal bovine serum (FBS) and 50 μg/mL each of penicillin, streptomycin, and neomycin (Invitrogen). The solid tumor xenograft model was developed by subcutaneous injection of 1×10^7 subconfluent cells in 100 μL Dulbecco's phosphate-buffered saline (DPBS) in the lower back of female athymic nude mice (8–10 weeks old; Harlan, Indianapolis, IN). The probe was evaluated in a total of 10 nude mice bearing tumors from 0.4 to 1.2 cm in diameter.

Confocal Microscopy

Tumor cells were grown on eight-chamber glass slides. Twenty-four hours later, the cells at 40 to 50% confluence were incubated with 25 μL of one of the following probes in 150 μL of medium without FBS and antibiotics. The probes included Tf^{NIR}-Lip^{NBD}-CA, Tf-Lip^{NBD}-dye, and dye alone. To visualize the cellular uptake of probe reporters, an NIR dye Alexa fluor 680 fluorophore was used to replace the CA in the preparation of Tf-Lip^{NBD}-dye probe at a concentration of 2 μL in a 200 μL total probe. Incubation was carried out for 5, 30, 60, and 120 minutes, separately. After PBS washing (three times), cells were fixed using 10% neutralized formalin for 10 minutes and cell nuclei were counterstained using 4′,6-diamidino-2-phenylindole dihydrochloride (DAPI) blue-fluorescence dye. Confocal images were acquired with a Zeiss LSM 510 Confocal Microscopy System (Carl Zeiss Inc, Thornwood, NY) using a 633 nm excitation line and emission LP 650 filter for Tf^{NIR} and Alexa fluor 680 fluorophore (red), 488 nm excitation line and emission BP 505 – 550 filter for Lip^{NBD} (green), and 364 nm excitation line and emission BP 385 – 470 filter for DAPI (blue). Following sequential excitation, red, green, and blue fluorescent images of the same cells were merged using the Zeiss *AIM* software for colocalization of the probe different reporters within cells.

In Vitro MRI and Optical Imaging

To quantify the cellular uptake of probe reporters, optical imaging and MRI of the cell pellets were performed. Similar numbers of tumor cells were seeded on 10 cm culture dishes for optical imaging and in 150 cm flasks for MRI. Cells grown to subconfluence were incubated with a 200 μL probe (in 3 mL medium) for 10 cm dishes and a 600 μL probe (in 10 mL medium) for 150 cm flasks. Differently labeled probes, such as Tf^{NIR}-Lip^{NBD}-CA, Tf-Lip^{NBD}-dye, Lip^{NBD}-dye, CA alone, and dye alone, were used. Incubation was carried out for 60 minutes. After PBS washing (three times), cells were collected using enzyme-free cell dissociation solution and adjusted to the same number. Cells were pelleted in microcentrifuge tubes by centrifugation. The cell pellets were quantified with respect to fluorescent intensity (FI) using the Xenogen IVIS 200 imaging system with excitation/emission filters at 679/702 nm for Tf^{NIR} and the Alexa fluor 680 fluorophore and at 464/531 nm for Lip^{NBD} measurement. Statistical analysis (Student's two-tailed *t*-test) of the FI for cells with different treatments was performed using Microsoft *Excel*. To obtain enough cells for MRI, cell pellets were pooled from five replicates. MRI was acquired using a Bruker 400 MHz NMR machine (Bruker-Biospin, Billerica, MA). A spin-echo (SE) imaging sequence was used to obtain T_1-weighted images. The imaging parameters were as follows: echo time (TE) = 11.416 milliseconds, repetition time (TR) = 500 milliseconds, number of averages = 4, field of view = 20 × 20 mm, matrix size = 256 × 128, and slice thickness = 2 mm. A fast imaging with steady-state precession sequence was used for T_1 measurement. The T_1 measurement parameters were as follows: TE = 1.5 milliseconds, TR = 3 milliseconds, number of averages = 8, number of frames = 16, number of segments = 32, inversion delay = 49.2 milliseconds, and inversion repetition = 2572.3 milliseconds. The MRIs were taken in the cross-sectional view of the microcentrifuge tubes. The central slice image, which was not influenced by the image distortion owing to the susceptibility effect from the air-pellet boundary, was used for signal intensity measurement. All analyses were performed using the Bruker image sequence analysis tools. All experiments were repeated at least three times. The representative data are presented.

In Vivo MRI and Optical Imaging

The animal was anesthetized using 2% isoflurane and positioned with the tumor at the center of the coil. The physiologic condition of the animals was monitored using a respiratory gating device during the scanning. The tumor was scanned in the perpendicular direction of the tumor and animal skin interface using a Bruker 400 MHz, 89 mm NMR spectrometer. After a search for overall image quality, imaging time, and probe- and CA-mediated contrast enhancement using different imaging sequences and parameters, a multislice multiecho T_1-weighted SE sequence was used for imaging studies, with a TR of 800 milliseconds, a TE of 11.4 milliseconds, and a slice

thickness of 1 mm. For each animal, a baseline image was first obtained; the tumors were then sequentially imaged at an interval of 10 minutes until 3 hours following intravenous injection of 200 μL of Tf^{NIR}-Lip^{NBD}-CA probe (containing 12 μL of Magnevist) through the tail vein. This was equivalent to two times the Magnevist dosage used in the clinic. For comparative study, the same animals were also imaged following intravenous administration of the same dosage of Lip-CA and CA alone (12 μL of Magnevist in 200 μL of pure water). The interval period between the two MRI studies was at least 3 days to avoid any influence of CA from the previous imaging study. The direction of the tumor was marked each time with water-filled small balls and marker pens before imaging. For optical imaging, the FI of tumors was monitored from 10 minutes after administration of the probe to 3 to 5 days using a Xenogen IVIS 200 imaging system.

Pathologic Analysis

After imaging, the mice were autopsied and the tumors were sampled, fixed in 10% neutral buffered formalin, and embedded in paraffin. Tumors were sectioned in the same direction as MRIs based on the markers of the tumor border made before MRI. Hematoxylin-eosin staining was used for pathologic examination. A comparison was performed between the tumor pathology and the image enhancement pattern in MRI.

Results

Visualization of Tf- and Lip-Mediated Cellular Uptake

For confocal microscopic observation of the cellular uptake of the probe reporters, cells were incubated with the probe Tf-Lip^{NBD}-dye or dye alone from 5 minutes to 2 hours. Here the probe was constructed using unlabeled Tf and NIR fluorescent dye instead of CA to visualize the uptake of encapsulated reagents within Lip. Figure 1 shows representative microscopic images. Both Lip^{NBD} (green) and fluorescent dye (red) were observed to be present in the cell cytoplasm as early as 5 minutes after incubation with the probe, and their FI within the cytoplasm increased gradually, reaching a maximum at about 1 hour of incubation (see Figure 1, A–C). Interestingly, the Lip^{NBD} and dye accumulated again, forming multiple endosomes. These endosomes were mainly located at the peripheral area of the cytoplasm and became more evident at 2 hours of incubation (see Figure 1, D–F), suggesting receptor-mediated endocytosis and release or degradation of the probe reporters through the action of lysosomal enzymes. Cellular uptake of the dye was not evident in the cells incubated with dye alone.

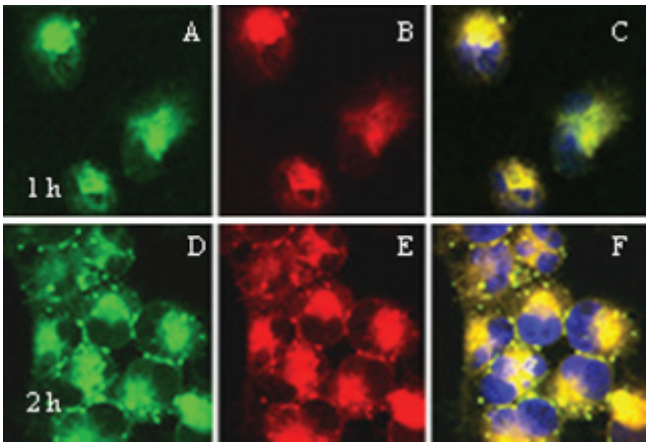

Figure 1. Confocal microscopic observation of cellular uptake of probe reporters. Cells were incubated with the probe transferrin-liposome-nitrobenzoxadiazole (Tf-Lip^{NBD})-dye for 5 minutes to 2 hours. *A* to *C* are representative images acquired at the 1 hour of incubation time point showing distribution and colocalization of Lip^{NBD} (*A*) and near-infrared (NIR) dye (*B*) in the cytoplasm. *D* to *F* are representative images acquired at the 2 hours of incubation time point showing multiple endosomes formed by Lip (*D*) and NIR dye (*E*) and colocalized in the peripheral area of the cytoplasm (*F*). Nuclei were counterstained using 4′,6-diamidino-2-phenylindole dihydrochloride (DAPI). Cells were imaged with a 63 × 1.4 NA Plan-Apochromat oil-immersion objective.

To visualize whether the Tf and Lip were co-internalized, confocal microscopy and optical imaging were performed for cells incubated with Tf^{NIR}-Lip^{NBD}-CA, Lip^{NBD}-CA, or CA alone. Similarly, from 5 minutes of incubation, the Tf^{NIR} (Figure 2A) and Lip^{NBD} (Figure 2B) were already colocalized within cell cytoplasm (Figure 2C). Optical imaging of the cell pellets further confirmed the uptake of the probe in tumor cells. To avoid membrane damage and probe leakage from cells, enzyme-free PBS-based cell dissociation solution was used instead of trypsin for cell dissociation from culture dishes. As shown in Figure 2D, only cells incubated with Tf^{NIR}-Lip^{NBD}-CA showed a strong fluorescent signal of Tf^{NIR}. Both cells incubated with Tf^{NIR}-Lip^{NBD}-CA and cells incubated with Lip^{NBD}-CA showed strong fluorescent signal of Lip^{NBD} (Figure 2E). Neither Tf^{NIR} nor Lip^{NBD} signal was detectable in cells incubated with CA alone.

We further evaluated whether the CA encapsulated within the probe was internalized into tumor cells using MRI of the cell pellets. A representative MRI of the cell pellets obtained from cells incubated with Tf^{NIR}-Lip^{NBD}-

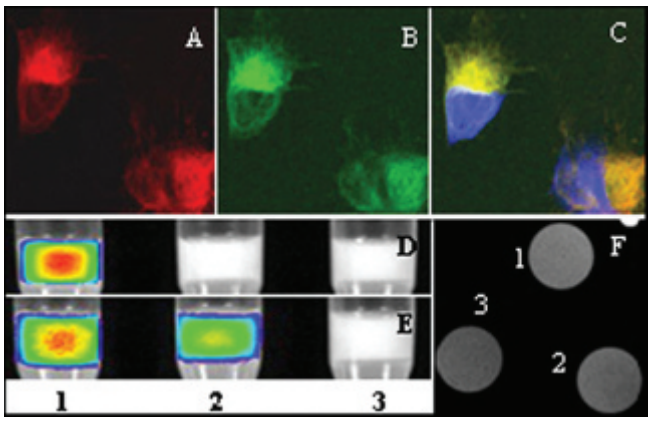

Figure 2. Confocal, optical, and magnetic resonance imaging (MRI) detection of the reporters in cells incubated with the probe near-infrared transferrin-liposome-nitrobenzoxadiazole-contrast agent (Tf^{NIR}-Lip^{NBD}-CA) for 1 hour. *A* to *C* are representative confocal microscopic images showing distribution and colocalization of Tf^{NIR} (*A*) and Lip^{NBD} (*B*) in cytoplasm. *D* to *E* are optical images of the cell pellets. A strong fluorescent signal of Tf is detected in cells incubated with Tf^{NIR}-Lip^{NBD}-CA (*D*, lane 1) but not in cells incubated with Lip^{NBD}-CA or with CA alone (*D*, lanes 2 and 3). Similarly, the strongest signal of Lip^{NBD} is detected in cells incubated with Tf^{NIR}-Lip^{NBD}-CA (*E*, lane 1) and less in cells incubated with Lip^{NBD}-CA (*E*, lane 2) but not in cells incubated with CA alone (*E*, lane 3). *F* shows the MRIs of the cell pellets. A stronger signal enhancement and T_1 shortening are obtained in cells incubated with Tf^{NIR}-Lip^{NBD}-CA and in cells incubated with Lip^{NBD}-CA (1 and 2) than in cells incubated with CA alone (3). The MRI parameters are as follows: echo time = 11.416 milliseconds, repetition time = 500 milliseconds, number of averages = 4, field of view = 20 × 20 mm, matrix size = 256 × 128, and slice thickness = 2 mm.

CA, Lip^{NBD}-CA, or CA alone is shown in Figure 2F. The corresponding signal intensity and T_1 relaxation time are shown in Table 1. Cells incubated with the probe Tf^{NIR}-Lip^{NBD}-CA or Lip^{NBD}-CA showed a much greater positive contrast and T_1 shortening than the cells incubated with CA alone. The T_1 relaxation time shortened from 408 milliseconds for CA alone to 374 milliseconds for Lip^{NBD}-CA and 366 milliseconds for Tf^{NIR}-Lip^{NBD}-CA ($p < .05$). The cells incubated with Tf^{NIR}-Lip^{NBD}-CA also showed higher signal intensity than the cells incubated with Lip^{NBD}-CA. These results highly indicate the importance and specificity of Tf moiety for targeting the probe internalization into tumor cells in vitro. The difference in signal intensity and T_1 relaxation time mediated by Lip^{NBD}-CA and by CA alone might reflect the effective fusion of Lip with tumor cell membrane.

Quantification of Tf- and Lip-Mediated Cellular Uptake

To evaluate the efficiency of Tf- and Lip-mediated cellular uptake, the FI of the Lip^{NBD} and NIR dye within the tumor cells was quantified following 1 hour's incubation of the cells with probes. The FI of NIR dye in the cells incubated with Tf-Lip^{NBD}-dye and with Lip^{NBD}-dye was more than 200-fold higher than that in the cells with dye alone (Table 2). Cells incubated with dye alone showed a similar level of FI to cells without probe and dye exposure (autofluorescence background). Approximately 1.5-fold higher FI of the intracellular NIR dye was observed in cells incubated with Tf-Lip^{NBD}-dye than in cells incubated with Lip^{NBD}-dye. Similarly, 2-fold higher FI of Lip^{NBD} was detected in cells incubated with Tf-Lip^{NBD}-dye or Lip^{NBD}-dye than in cells incubated with NIR dye alone (autofluorescent background) (see Table 2). The FI of Lip^{NBD} was 1.3-fold higher in cells incubated with Tf-Lip^{NBD}-dye than in cells incubated with Lip^{NBD}-dye. Student's *t*-tests (two-tailed)

Table 1. Comparison between Probe- and Contrast Agent–Mediated Signal Enhancement

MRI Measurement	*Tf^{NIR}-Lip^{NBD}-CA*	*Lip^{NBD}-CA*	*CA Alone*
Relative intensity (10^5)	17.7 ± 0.86	15.33 ± 0.86	13.25 ± 0.78
T1 relaxation time (ms)	366.7 ± 17.1	374.3 ± 17.3	408.1 ± 13.8

CA = contrast agent; Lip = liposome; NBD = nitrobenzoxadiazole; NIR = near-infrared; Tf = transferrin.
$p < .05$ between probe and CA alone for both relative intensity and T_1.

Table 2. Optical Quantitation of Probe-Mediated Cellular Uptake of Reporters

Reporters	*Tf-Lip^{NBD}-Dye*	*Lip^{NBD}-Dye*	*Dye Alone*
NIR dye (× 10^9)	6.88 ± 0.59	4.99 ± 0.51	0.23 ± 0.006
Lip^{NBD} (× 10^7)	2.03 ± 0.14	1.64 ± 0.09	1.10 ± 0.13

Lip = liposome; NBD = nitrobenzoxadiazole; NIR = near-infrared; Tf = transferrin.
$p < .05$ between probe and dye alone and also between Tf-Lip^{NBD} dye and Lip^{NBD} dye for both dye and Lip^{NBD} uptake. Quantitation is based on the fluorescence intensity (p/s/cm^2/sr) of cell pellets.

between cells incubated with probe and with dye alone for both intracellular Lip^{NBD} and NIR dye intensity were both significantly different ($p < .05$). The FI in cells incubated with Tf-Lip^{NBD}-dye and in cells incubated with Lip^{NBD}-dye was also significantly different ($p < .05$) for both intracellular Lip^{NBD} and NIR dye uptake.

To further test the specificity of Tf-mediated cellular uptake, cells were first pretreated for 1 hour with unlabeled Tf before incubation with the probes. The amount of Tf was threefold (375 μg/dish) higher than that used in the probe (125 μg/dish). Following incubation with the probe Tf-Lip^{NBD}-dye, the FI of the NIR dye in cells with and without Tf pretreatment was 2.45×10^9 and 3.42×10^9 p/s/cm^2/sr, respectively (Table 3). The FI of the Lip^{NBD} in cells with and without Tf pretreatment was 2.57×10^7 and 3.45×10^7 p/s/cm^2/sr, respectively. Calculation based on the control cells incubated with Lip^{NBD}-dye revealed a blockage of 65.6% of the dye uptake and 70.97% of the Lip^{NBD} uptake by Tf pretreatment. These results indicate that the probe reporter uptake in vitro was mediated by both Tf and cationic Lip. Tf and Lip have an apparent synergistic effect on the cellular uptake of the probe reporters.

Probe-Mediated Signal Enhancement of the Tumors In Vivo

Signal enhancement was evaluated in 10 athymic nude mice with solid tumor xenografts. The tumor size ranged from 0.4 to 1.2 cm in diameter. To compare the signal enhancement mediated by the probe and mediated by the CA alone, the same mice were used for the probe and CA-alone studies sequentially with an interval of at least 3 days. Intravenous administration of the probe Tf^{NIR}-Lip^{NBD}-CA significantly enhanced the tumor image contrast (Figure 3). The enhancement was observed as early as 10 minutes after administration and increased gradually, reaching the maximum at 90 minutes to 2 hours. After that, a gradual decrease in the signal enhancement was observed. Interestingly, the enhancement was greatly heterogeneous within the tumors (see Figure 3). The enhancement pattern became relatively consistent from 1 to 3 hours. Some areas of the tumors were strongly enhanced initially, whereas other areas were weakly enhanced. The signals from the strongly enhanced region decreased much more slowly than the signals from the region with weak enhancement. For small tumors, the enhancement was relatively uniform and the enhancement was usually observed starting from the peripheral area. Magnevist alone slightly enhanced the image contrast of tumors compared with the baseline images (Figure 4). The maximum enhancement was usually observed at 30 to 60 minutes after injection. The image contrast enhancement started from the peripheral area to the center of the tumors and was relatively uniform within tumors irrespective of the sizes studied here. The signal enhancement decreased rapidly and returned to baseline within 3 hours. The pharmacokinetics of pure Magnevist was different from that of Tf-labeled Magnevist containing Lip. Magnevist containing Lip without linkage to Tf showed a much weaker signal enhancement than either CA alone or Tf^{NIR}-Lip^{NBD}-CA.

Detection and Dynamic Change of the Fluorescent Signal in Tumors In Vivo

To understand whether the probe was preferentially accumulated in tumors and whether the fluorescent signal was optically detectable in vivo, tumors were monitored using Tf^{NIR}-based optical imaging. The fluorescent signal was clearly detectable as early as 10 minutes and reached the maximum intensity at about 90 minutse to 2 hours after intravenous injection of the probe Tf^{NIR}-Lip^{NBD}-CA (Figure 5). The FI was related to the tumor sizes, and significant FI was still detectable after 2 days for larger tumors (usually > 0.8 cm in diameter). The FI of smaller tumors became very weak at 24 hours. The FI of Lip^{NBD} was too weak to be detectable by optical imaging in vivo, although it was clearly detected ex vivo. High background fluorescence was another reason for the failure to detect Lip^{NBD} in tumors. Following intravenous injection, the probe was rapidly distributed throughout the body and

Table 3. Blockage of Transferrin-Mediated Uptake of Reporters by Transferrin Pretreatment

Reporters	*Tf-Lip^{NBD}-Dye*	*Tf-Lip^{NBD}-Dye*	*Lip^{NBD}-Dye*
NIR dye ($\times 10^9$)	3.42 ± 0.17	2.45 ± 0.21	1.94 ± 0.20
Lip^{NBD} ($\times 10^7$)	3.45 ± 0.29	2.57 ± 0.21	2.21 ± 0.16

Lip = liposome; NBD = nitrobenzoxadiazole; NIR = near-infrared; Tf = transferrin.
$p < .05$ between pretreated and untreated cells for both dye and Lip^{NBD} uptake. Quantitation is based on the fluorescence intensity (p/s/cm^2/sr) of cell pellets.

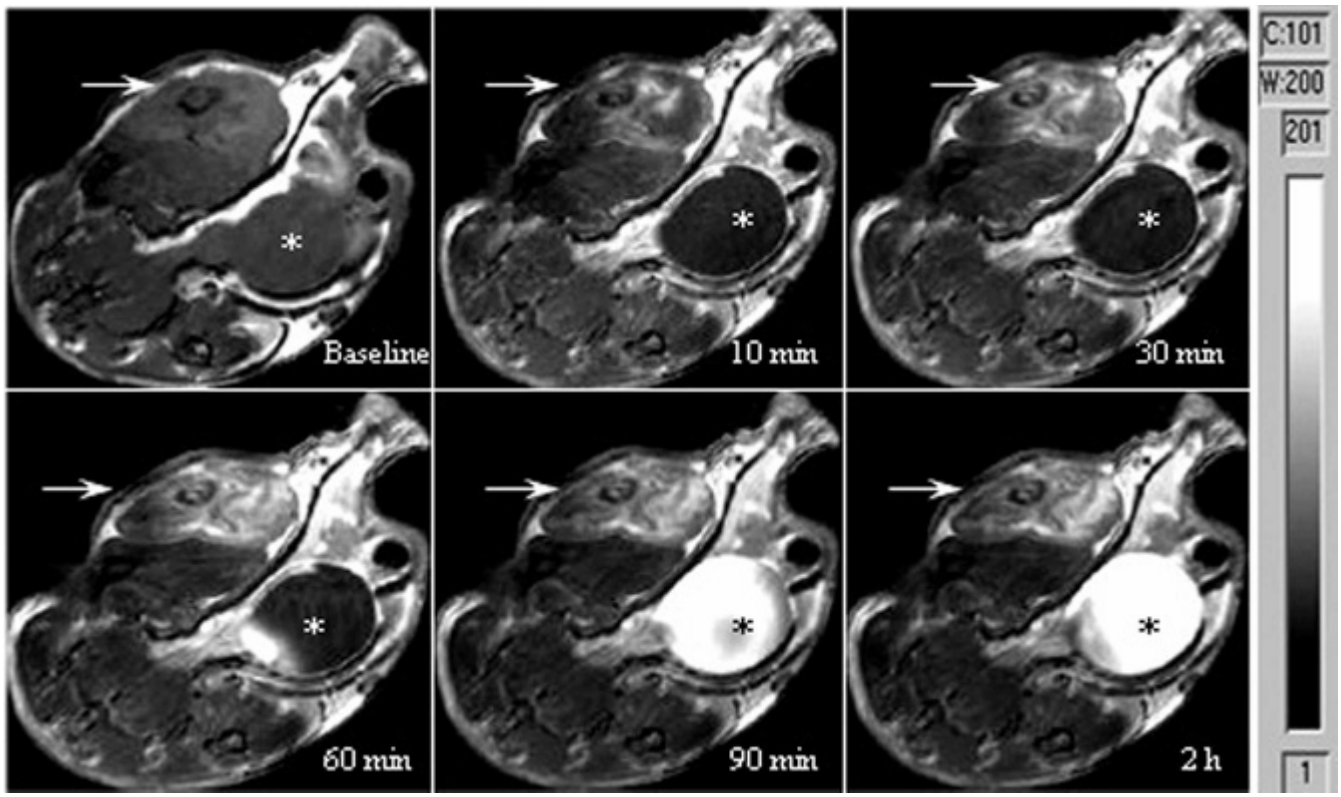

Figure 3. In vivo time course of tumor magnetic resonance imaging (MRI) after intravenous administration of the probe transferrin-liposome-nitrobenzoxadiazole-contrast agent (Tf^{NIR}-Lip^{NBD}-CA) showing gradually increased enhancement of the tumor signal (*arrow*) and a heterogeneous enhancement pattern. Gradual accumulation of contrast agent in the urinary bladder is evident (*). The MRI parameters are as follows: echo time = 11.416 milliseconds, repetition time = 800 milliseconds, number of averages = 4, field of view = 28 × 30 mm, matrix size = 256 × 192, and slice thickness = 1.0 mm.

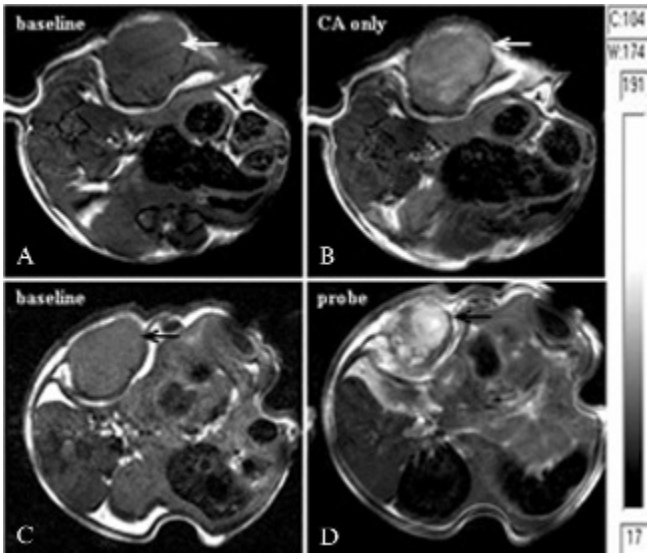

Figure 4. Comparison of the signal enhancement by contrast agent (CA) alone (*A–B*) and by the probe transferrin-liposome-nitrobenzoxadiazole-contrast agent (Tf^{NIR}-Lip^{NBD}-CA) (*C–D*). The magnetic resonance images (MRIs) are from the same tumor, with an interval of 72 hours between studies with the probe and with CA alone. A stronger, heterogeneous signal enhancement is achieved with Tf^{NIR}-Lip^{NBD}-CA over CA alone. The MRI parameters are the same as for Figure 3.

was first taken up by the well-perfused organs, such as the liver, spleen, lung, and bone marrow. However, the probe was rapidly washed out from these organs but not from solid tumors. The uptake of the probe in tumors was enhanced because of binding to TfR in the tumor. After the initial rapid increase in the background fluorescence following injection of the probe, the background fluorescence decreased rapidly, as shown in Figure 5H. The tumor to normal (contralateral muscle) ratio varied from 1.3 to 3.4 at the different time points following injection (from 10 minutes to 48 hours), which was related to the tumor sizes. Small tumors (less than 3 mm in diameter) showed less fluorescent signal, perhaps owing to differences in vasculature. Similar to the MRI finding, fluorescent dye containing Lip without Tf linkage failed to induce a preferential increase in fluorescent signal in tumors.

Comparison between MRI Signal Enhancement and Pathologic Findings

To understand the underlying mechanism of heterogeneous contrast enhancement within the tumors by the

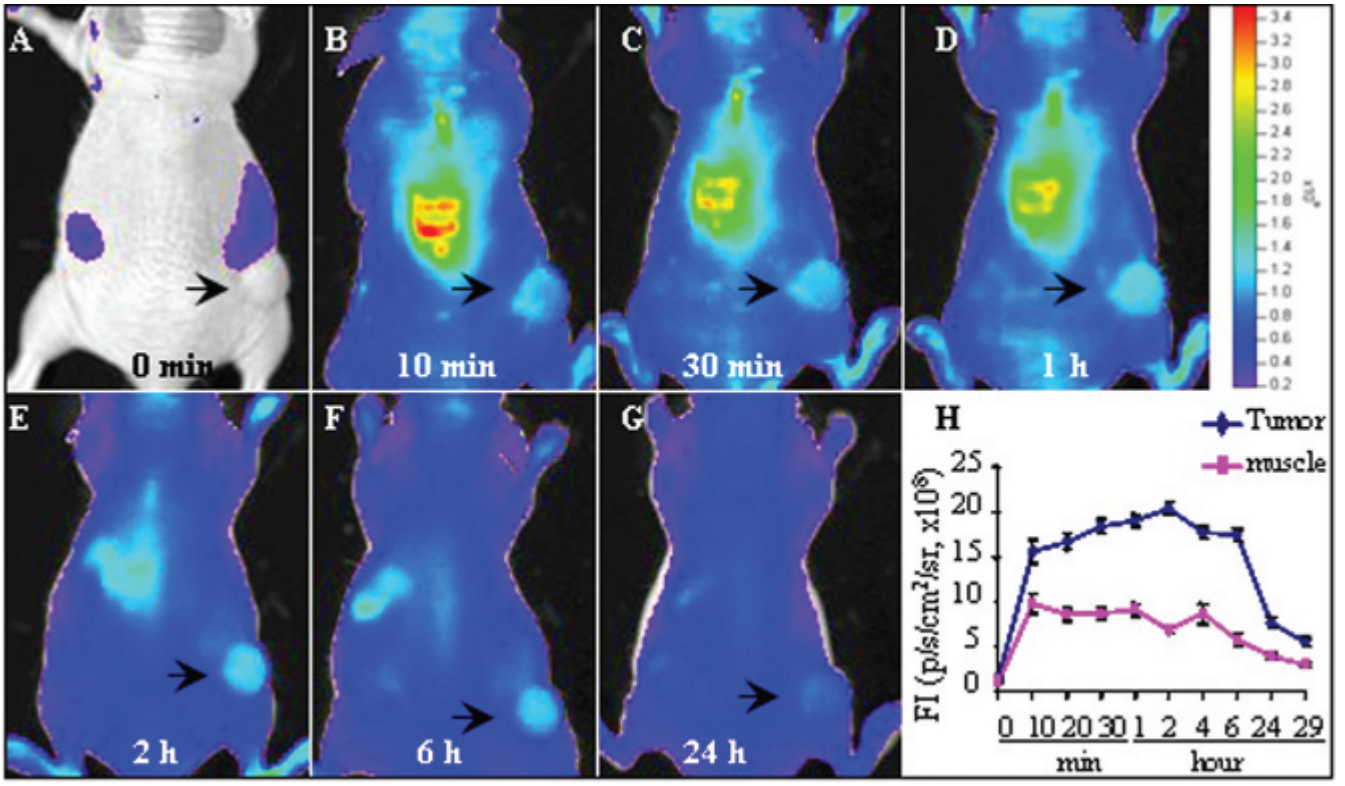

Figure 5. Optical imaging of the tumor after intravenous administration of transferrin-liposome-nitrobenzoxadiazole-contrast agent (Tf^{NIR}-Lip^{NBD}-CA) showing preferential accumulation of fluorescent signal in tumors (*A–G*). The fluorescence signal was detectable as early as 10 minutes and reached a maximum at about 2 hours and then deceased gradually. *H* shows the plot of time versus signal intensity obtained from the tumor and the contralateral muscle. The signal intensity is expressed as p/s/cm^2/sr.

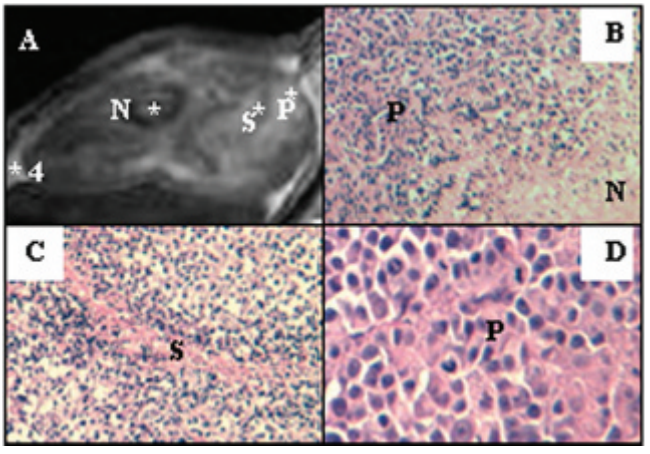

Figure 6. Correlation of magnetic resonance imaging (MRI) with pathologic findings showing high consistency between the probe-mediated enhancement pattern in MRI and pathologic findings (hematoxylin-eosin stain). *A* is a representative MRI (same as Figure 3) showing a heterogeneous enhancement pattern. *B* shows a region with high proliferation and necrosis (×250 original magnification). *C* shows the stromal tissue (×250 original magnification), and *D* shows the proliferating tumor cells with high mitotic activity (×400 original magnification). N = necrosis; P = proliferating cells; S = stromal tissue.

probe, a comparative analysis was performed between MRI signal enhancement and pathologic findings (Figure 6). Pathologically, the tumor cells in large tumors with heterogeneous enhancement usually presented various stages of growth and necrosis. In some areas, the tumor cells were completely necrotized and became amorphous and liquefied. In some other regions, the tumor cells showed dying features such as condensed or broken nuclei or only shadow cells remaining. The highly enhanced regions of the tumors in MRIs represented the more actively proliferating tumor cells, whereas the weakly enhanced areas contained less active or dying cells. The completely necrotized region showed the least enhancement. The heterogeneous signal enhancement by the probe was well correlated with the in vivo morphologic features of the tumors.

Discussion

The human Tf-targeted cationic Lip—deoxyribonucleic acid (DNA) complex has been used for efficient gene

transfer in animal models recently. The formulation for optimal transfection of cancer cells has been optimized as a DNA:lipid:Tf ratio of 1 μg:10 nmol:12.5 μg with Lip composition of DOTAP:DOPE (1:1, w/w). This complex of Tf-Lip-DNA demonstrates a highly compact structure that resembles a virus particle with a dense core enveloped by a membrane coated with Tf molecules spiking the surface.[20,21] Successful gene delivery using Tf-targeted cationic Lip is based on the fact that TfR is overexpressed in various malignant tumors and Tf-TfR-mediated endocytosis is highly efficient. Furthermore, cationic Lip has many advantages, such as high encapsulation capacity, much less immunogenicity and toxicity, and dramatically increased transfection efficiency through linkage with ligands.[22] These characteristics of this system also fulfill the criteria for an ideal system for molecular imaging in vivo. Using the advantages of this system, we developed the probe with both NIR fluorescence and MRI reporters, which is suitable for both optical and nuclear MRI.

Use of the NIR fluorescence molecule minimizes the autofluorescence interference from healthy tissue and allows the visualization of tissues millimeters in depth because of efficient penetration of photons in the NIR range.[11,12] To encapsulate the CA, we directly hydrated the dried Lip films with concentrated CA solution and downsized the Lip-CA complex by sonication and repeated passing through the membrane before linkage with Tf. The Lip:Tf ratio (10:12.5) used in the probe was optimized as reported previously.[20–24] The dosage of Magnevist was 0.2 mmol/kg, corresponding to two times the recommended dose for the patient. For this amount of Magnevist (even threefold more), almost all of the Magnevist was found to be encapsulated within the Lip, as estimated by gel filtration and fluorescence study. Our previous study also confirmed Magnevist encapsulation within Lip using scanning electron microscopy and scanning probe microscopy.[25] The Tf, cationic Lip, and Gd complex was coupled through charge interaction, which makes the preparation of the probe simple enough to be freshly prepared before use. A concern for Lip carrier, as in the gene delivery, is its size. It has been reported that linkage with Tf condenses the Lip-DNA complex with a uniform size of 50 to 90 nm.[20,23] After sonication of the probe, we found that repeated passing through 200 and 100 nm polycarbonate membranes resulted only in a loss of less than 10% of the probe and the majority of the probe particles were within 100 nm in size based on the fluorescence measurement of the probe. Transportation of the probe across tumor vessels occurs via open gaps, vesicular vacuoles, and/or fenestrations. A characteristic pore cutoff size is measured ranging from 200 nm to 1.2 μm in tumors.[26] Another analysis points out that the pore cutoff size is around 400 nm based on in vivo fluorescence microscopy studies of the transportation of sterically stabilized Lip into solid tumors.[27] Therefore, the size of our probe should not be a limitation to transport from tumor vasculature into tumor cells.

We first evaluated the probe-mediated uptake efficiency of the reporters in vitro. To visualize and quantify the efficiency, the components of the probe were differentially labeled. On confocal microscopy, Tf^{NIR}, Lip^{NBD}, and the encapsulated NIR dye were clearly codistributed within the cytoplasm of tumor cells. They accumulated and formed endosomes again in the peripheral area of the cytoplasm. In Tf-Lip-mediated plasmid DNA transfection, similar endosome formation has been reported by Lee and Kim.[28] They also found nuclear localization of the Tf-Lip. In our system, no nuclear signal of the probe was observed. Quantitative analysis using optical imaging further confirmed the finding of confocal microscopy. The cellular uptake was mediated by both Tf and Lip. Blockage of the TfR with Tf led to significantly decreased uptake. The possibility of nonspecific binding to free NIR dye was excluded because no fluorescent signal of the dye was detected in cells incubated with dye alone. Higher cellular uptake of the Lip and dye in cells incubated with Lip^{NBD}-dye without Tf linkage than in cells incubated with dye alone is not surprising. The probe reporters are taken up in vitro by two different pathways. One is due to Lip-mediated endocytosis and membrane fusion process because Lip is an effective transfection reagent.[22] The other is due to binding to TfR. The pretreatment with Tf is not expected to prevent endocytosis of the probe reporters owing to Lip fusion with the cell membrane. Importantly, Tf and Lip showed a synergistic effect on the probe uptake by cells based on our quantitative and blocking analysis. MRI of the cell pellets revealed a similar finding that CA is internalized and the internalization is mediated by both Tf and Lip. The apparent synergistic effect may be explained by a three-step mechanism. The important first step is the specific binding of Tf with TfR on the cell surface followed by the interaction of cationic Lip with anionic cell membrane and finally the receptor- and Lip-membrane fusion-mediated endocytosis.[29]

For MRI study, a T_1-weighted imaging technique was used to evaluate the positive contrast enhancement mediated by our probe. The actual T_1 shortening in vivo depends on the accumulation of the probe in time, which, in turn, depends on tumor physiology. We have searched the best imaging strategy by using different imaging

sequences and by varying the imaging parameters. The choice of SE sequence with TR = 800 milliseconds and TE = 11.4 milliseconds was based on the consideration of overall image quality, imaging time, and the differences of contrast enhancement between the probe and CA-alone studies. Consistent with our in vitro findings, specific targeting of the probe in vivo was demonstrated by both optical imaging and MRI. A preferential accumulation of the fluorescent signal in tumors and a significant signal enhancement are clearly achieved with the dual probe but not with CA alone. Time course study revealed a high consistency among confocal images, optical fluorescence, and MRI contrast enhancement. The maximum signal enhancement and FI in tumors are seen at ≈90 minutes, and both reach a plateau (which includes the maximum) between 1 and 3 hours after intravenous injection, whereas the maximal magnetic resonance contrast enhancement is achieved at about 45 minutes following administration of CA alone and the enhancement reduces to baseline within 3 hours. The magnetic resonance signal enhancement achieved by the dual probe is much stronger than that achieved by the CA alone. These results are consistent with the finding in gene therapy using a Tf-mediated Lip system that high gene transfection efficiency is observed within tumors.[23,24] More interestingly, heterogeneous enhancement in MRIs is evident in large tumors, which correlates well with the histologic findings. Within the range of tumor sizes in the present study, CA alone could enhance the image contrast, but the enhancement was weak and relatively uniform. Heterogeneous enhancement that could be correlated with histology may be potentially valuable. It makes it possible to interpret the pathologic features based on specifically enhanced MRI. More information could be provided to the clinician without further invasive procedure of biopsy.[3,30] In vivo, significant uptake of the probe reporters was not observed in the case of Magnevist or fluorescent dye containing Lip without linkage to Tf. This may be explained by the fact that the majority of the Lip accumulated within well-perfused organs, such as the liver, spleen, bone marrow, and lung. The uptake and retention of Magnevist or fluorescent dye containing Lip were very low in tumors. This is in contrast to the uptake of Lip bound to Tf. Positive CA may be superior to the negative CA, such as an iron oxide probe. A decrease in the image intensity by negative CA will complicate interpretation of tumor necrosis and poor expression of target receptors. The advantages of using a superparamagnetic Tf-labeled iron oxide probe are the small size and long-range T_2 effect. Because of the long-range T_2 effect, it requires less compound for a greater image intensity change. Our probe can be used for optical detection of tumors and is potentially useful for imaging the expression level of TfR and tumor cell growth. These parameters are of great value in predicting the prognosis and treatment selection. This goal can be achieved by measuring the intensity of fluorescence in optical images. However, limited penetration of fluorescence is still a problem, particularly for deep organ tumors. Clearly, use of multimodality reporter constructs can overcome many of the shortcomings of each modality alone.[14,15]

In conclusion, we have described a novel nano-sized molecular probe with both optical and MRI reporters. In vitro and in vivo analysis confirmed the probe specificity, internalizing efficiency, and sufficiency for multimodality detection. In MRI, the probe significantly enhances the tumor contrast so that it can increase the sensitivity to detect small tumors. The tumor enhancement pattern could help evaluate the pathologic features of tumors in vivo, which provides more information for the clinician. Preferential accumulation of the probe NIR fluorescence makes the tumor detectable using NIR-based optical imaging. Furthermore, it provides the possibility of quantifying the specific biomarkers expressed in tumors, which will be helpful to determine the patient's prognosis and response to treatment.

Acknowledgments

We thank Dr. Elizabeth G. Snyderwine and Dr. Minshu Yu (Laboratory of Experimental Carcinogenesis, National Cancer Institute [NCI], NIH) for their scientific advice. We are grateful to Stephen M. Wincovitch and Susan H. Garfield (CCR Confocal Microscopy Core Facility, NCI, NIH) for help and consultation with confocal microscopy.

References

1. Pautler RG. Mouse MRI: concepts and applications in physiology. Physiology 2004;19:168–75.
2. Artemov D. Molecular magnetic resonance imaging with targeted contrast agent. J Cell Biochem 2003;90:518–24.
3. Massoud TF, Gambhir SS. Molecular imaging in living subjects: seeing fundamental biological processes in a new light. Gene Dev 2003;17:545–80.
4. Persigehl T, Heindel W, Bremer C. MR and optical approaches to molecular imaging. Abdom Imaging 2005;30:342–54.
5. Blasberg RG. Molecular imaging and cancer. Mol Cancer Ther 2003;2:335–45.
6. Funovics MA, Kapeller B, Hoeller C, et al. MR imaging of the her2/neu and 9.2.27 tumor antigens using immunospecific contrast agents. Magn Reson Imaging 2004;22:843–50.

7. Basilion JP. Current and future technologies for breast cancer imaging. Breast Cancer Res 2001;3:14–6.
8. Artemov D, Mori N, Okollie B, Bhujwalla ZM. MR molecular imaging of HER-2/neu receptor in breast cancer cells using targeted iron oxide nanoparticles. Magn Reson Med 2003;49:403–8.
9. Mulder WJM, Strijkers GJ, Griffioen AW, et al. A liposomal system for contrast-enhanced magnetic resonance imaging of molecular targets. Bioconjugate Chem 2004;15:799–806.
10. Graves EE, Weissleder R, Ntziachristos V. Fluorescence molecular imaging of small animal tumor models. Curr Mol Med 2004;4:419–30.
11. Ntziachristos V, Bremer C, Weissleder R. Fluorescence imaging with near-infrared light: new technological advances that enable in vivo molecular imaging. Eur Radiol 2003;13:195–208.
12. Hoffman RM. The multiple uses of fluorescent proteins to visualize cancer in vivo. Nature 2005;5:796–806.
13. Schellenberger EA, Sosnovik D, Weissleder R, Josephson L. Magneto/optical annexin V, a multimodal protein. Bioconjugate Chem 2004;15:1062–7.
14. Blasberg RG. In vivo molecular-genetic imaging: multi-modality nuclear and optical combinations. Nucl Med Biol 2003;30:879–88.
15. Veiseh O, Sun C, Gunn J, et al. Optical and MRI multifunctional nanoprobe for targeting gliomas. Nano Lett 2005;5:1003–8.
16. Jones DT, Trowbridge IS, Harris AL. Effects of transferrin receptor blockade on cancer cell proliferation and hypoxia-inducible factor function and their differential regulation by ascorbate. Cancer Res 2006;66:2749–56.
17. Hogemann-Savellano D, Bos E, Blondet C, et al. The transferrin receptor: a potential molecular imaging marker for human cancer. Neoplasia 2003;5:495–506.
18. Xu L, Pirollo KF, Tang WH, et al. Transferrin-liposome-mediated systemic p53 gene therapy in combination with radiation results in regression of human head and neck cancer xenographs. Hum Gene Ther 1999;10:2941–52.
19. Bellocq NC, Pun SH, Jensen GS, Davis ME. Transferrin-containing, cyclodextrin polymer-based particles for tumor-targeted gene delivery. Bioconjugate Chem 2003;14:1122–32.
20. Xu L, Frederik P, Pirollo KF, et al. Self-assembly of a virus-mimicking nanostructure system for efficient tumor-targeted gene delivery. Hum Gene Ther 2002;13:469–81.
21. Kursa M, Walker GF, Roessler V, et al. Novel shielded transferring-polyethylene glycol-polyethylenimine/DNA complexes for systemic tumor-targeted gene transfer. Bioconjugate Chem 2003;14:222–31.
22. Simoes S, Pires P, Duzgunes N, Pedroso de Lima M. Cationic liposomes as gene transfer vectors: barriers to successful application in gene therapy. Curr Opin Mol Theory 1999;1:147–57.
23. Nakase M, Inui M, Okumura K, et al. p53 gene therapy of human osteosarcoma using a transferring-modified cationic liposome. Mol Cancer Ther 2005;4:625–31.
24. Pirollo KF, Xu L, Chang EH. Non-viral gene delivery for p53. Curr Opin Mol Ther 2002;2:168–75.
25. Pirollo K, Dagata J, Wang P, et al. A tumor-targeted nanodelivery system to improve early MRI detection of cancer. Mol Imaging 2006;5:41–52.
26. Hobbs SK, Monsky WL, Yuan F, et al. Regulation of transport pathways in tumor vessels: role of tumor type and microenvironment. Proc Natl Acad Sci U S A 1998;95:4607–12.
27. Unezaki S, Maruyama K, Hosoda JI, et al. Direct measurement of extravasation of poly-ethyleneglycol-coated liposomes into solid tumor tissue by in vivo fluorescence microscopy. Int J Pharm 1996;144:11–7.
28. Lee SM, Kim JS. Intracellular trafficking of transferring-conjugated liposome/DNA complexes by confocal microscopy. Arch Pharm Res 2005;28:93–9.
29. Yin J, Lin AJ, Buckett PD, et al. Single-cell FRET imaging of transferrin receptor trafficking dynamics by sfp-catalyzed, site-specific protein labeling. Chem Biol 2005;12:999–1006.
30. Mankoff D. Imaging in breast cancer—breast cancer imaging revisited. Breast Cancer Res 2005;7:276–8.

Running title
Bioluminescent Animal Models of Breast Cancer

Title
Bioluminescent Animal Models of Human Breast Cancer for Tumor Biomass Evaluation and Metastasis Detection

Liang Shan[1], M.D., Ph.D., Songping Wang[1], Ph.D. Alexandru Korotcov[1], Ph.D., Rajagopalan Sridhar[2], Ph.D. and Paul C. Wang[1], Ph.D.

[1]Department of Radiology, [2]Department of Radiation Oncology, Howard University, Washington DC, USA

Correspondence: Paul C. Wang, Ph.D.
Department of Radiology, Howard University
2041 Georgia Ave, N.W., Washington DC 20060
Tel: 202-865-3711, Fax: 202-865-3722,
E-mail: pwang@howard.edu

Word count: Abstract: 247 Words of Text: 1827
Number of figures: 3 Number of tables: 0
Number of references: 16

Abstract

Introduction: There is a need for convenient animal models for studying the progress of human tumors in vivo. Luciferase-based bioluminescent imaging (BLI) enables tumor monitoring noninvasively and is sensitive to subtle changes in tumors.

Methods: Three human breast cancer models in nude mice were established using luciferase-expressing MDA-MB-231-luc cells. They were subcutaneous xenografts (n=8), mammary gland xenografts (n=5) and lung metastasis (n=3). The tumors were imaged in live mice using a highly sensitive BLI system. The relationship between the intensity of bioluminescence from the tumor was analyzed with respect to tumor volume. Bioluminescent signal from lung metastasis was studied in order to determine the threshold of detectability.

Results: Tumors growing in the mouse backs and mammary gland fat pads were imaged dynamically following administration of D-luciferin. The bioluminescent intensity from the tumors gradually increased and then decreased over time within 1 hour. The time to reach maximum signal intensity differed significantly among tumors, and was independent of tumor volume and unrelated to maximum signal intensity. A significant correlation was observed between tumor volume and maximum signal intensity in tumors from both sites. Lung metastatic lesions of 0.3-0.5 mm in diameter could be clearly detected through whole animal imaging.

Conclusion: The animal models established using luciferase-expressing cancer cells in combination with BLI provide a system for rapid, non-invasive and quantitative analysis of tumor biomass and metastasis. This biosystem simplifies in vivo monitoring of tumors and will be useful for noninvasive investigation of tumor growth and response to therapy.

Keywords
Bioluminescent imaging, luciferase, animal models, breast cancer

Introduction

Bioluminescent imaging (BLI) is an optically based imaging method that enables rapid in vivo analyses of a variety of cellular and molecular events with extreme sensitivity (1-3). The imaging is based on the use of light-emitting enzymes such as luciferase as internal biological light sources that can be detected externally as biological indicators. As a result of recent developments in techniques for high sensitivity detection of bioluminescence, BLI has been recently tested in the detection and real time observation of primary tumor growth and metastasis in living subjects (4-6). Luciferase-based light emitting animal models have also been used for the development of therapeutics that targets the molecular basis of disease (7). Importantly, BLI provides a biosystem to test the spatio-temporal expression patterns of both target and therapeutic genes in living animals where the contextual influences of whole biological systems are intact (8, 9). In the present study, we established three bioluminescent animal models of human breast cancer using MDA-MB-231-luc cell line, which has a stably transfected with luciferase gene. The primary and metastatic lesions were analyzed through whole animal imaging and the tumor volume was evaluated in relationship with the bioluminescent signal intensity.

Materials and Methods

Cell culture and Animal models

MDA-MB-231-luc human breast cancer cell line and D-luciferin were obtained from Xenogen (Alameda, CA). This cell line has been stably transfected with luciferase gene for luciferase-based BLI. Cells were routinely maintained in DMEM/F-12 medium supplemented with 10% heat inactivated fetal bovine serum (FBS) and 50 µg/ml each of penicillin, streptomycin and neomycin (Invitrogen, Carlsbad, CA). Female athymic nude mice of 8-10 weeks of age (n=16) were purchased from Harlan (Indianapolis, IN). Three animal models were developed. The subcutaneous solid tumor xenograft model was developed by subcutaneous injection of $1x10^7$ subconfluent cells in 100 µl Dulbecco's phosphate buffered saline (DPBS) in the right lower back of mouse (n=8). The mammary gland fat pad tumor model was developed by injection of $1x10^7$ subconfluent cells in 100 µl DPBS in the right fifth mammary gland fat pad (n=5). The lung metastasis model of breast cancer was developed by tail vein injection of $1x10^6$ tumor cells (n=3). The tumors in subcutaneous tissue and mammary gland fat pad were imaged and analyzed when they reached a certain size (ranging from 3 to 11 mm in diameter). For lung metastatic model, whole animals were checked every week and autopsied when tumor signal from the lung region was detected.

In vivo BLI

Luciferase-based BLI was performed with a highly sensitive, cooled CCD camera mounted in a light-tight specimen box (Xenogen IVIS 200 imaging system). Imaging and quantification of signals were controlled by the acquisition and analysis software living

Image (Xenogen). Mice were placed onto the warmed stage inside the light-tight camera box with continuous exposure to 2% isoflurane. After a baseline image was taken, animals were given the substrate D-luciferin by intraperitoneal injection at 150 mg/kg in DPBS. The whole animal was imaged dynamically at an interval of 2 minutes (min) over 1 hour (hr). Imaging time was 1 min. The light emitted from the mouse was detected, integrated, digitized and displayed by the IVIS^{TM} camera system. Regions of interest from displayed images were identified and measured around the tumor sites. The signal was quantified and expressed as photons per second, (p/s) using Living Imaging® software (Xenogen).

All animal protocols were conducted according to NIH guidelines for humane use and care of animals. The animal protocols were approved by the institutional animal care and use committee of Howard University.

Histopathology

To confirm whether the detected signal from whole animal imaging originated from the metastatic lesions in the lung, the animal was autopsied as soon as the signal was detected. Lung was examined and fixed by intrabranchial perfusion of 10% neutralized formalin solution. Paraffin-embedded sections were stained using hematoxylin and eosin (HE) for microscopic evaluation.

Statistical analysis

Statistical analysis was performed using statistical software OriginPro 7.0 (OriginLab, Northampton, MA). A P-value of <0.05 was considered to be a significant difference between any two sets of data.

Results

Individual difference in dynamics of tumor bioluminescent signals

Eight tumors in the subcutaneous tissue in the backs and 5 tumors in the mammary gland fat pads of athymic nude mice were analyzed, separately. The maximum diameter of the 13 tumors ranged from 3 to 11 mm. Following administration of D-luciferin, the bioluminescent signal in tumors was clearly detectable as early as 2 min and showed a dynamic change of gradual increase and then decrease over time (Fig. 1). In majority of the tumors, the signal became very weak or undetectable within 60 min. There was a significant difference among tumors for the peak time, ranging from 5 to 24 min (defined as the time for luminescence intensity of tumor to reach the maximum). Similar phenomenon was observed for tumors located in the backs and mammary fat pads. There was no correlation between the peak time and tumor volume ($R=-0.13$, $P=0.76$ in subcutaneous tissue and $R=0.67$, $P=0.21$ in mammary gland). There was also no correlation between the peak time and maximal tumor signal intensity ($R=-0.18$, $P=0.67$ in subcutaneous tissue and $R=0.74$, $P=0.15$ in mammary gland). These results indicate that the dynamic change of tumor bioluminescent signal following D-luciferin administration might be related to mouse individual difference, independent of the tumor itself.

Close correlation between bioluminescent signal intensity and tumor volume

Because of the significant difference in the dynamics of tumor bioluminescent signals among mice, the maximal tumor signal measured at the peak time point was selected for further analysis. There was a significant correlation between the maximal signal and the tumor volume for tumors located at both mammary gland fat pad (R=0.90, P=0.035, Fig. 2A) and subcutaneous tissue (R=0.85, P=0.007, Fig. 2B). This result indicates that the bioluminescent signal intensity reflects the tumor size. The maximal signal intensity could be used as an indicator of tumor growth. The background signal was at a negligible level and significantly less than the signal from the tumor (Fig.1).

Highly sensitive in vivo detection of lung metastatic lesions

In three mice, the tumor cells were injected through tail vein and whole animal imaging was performed every week. Clear signal of tumor was first detected at lung area at about 1 month following tail vein injection of tumor cells. After recording the images, the mouse was autopsied immediately and the lung was examined pathologically. In one mouse, two distinct tumor signals were observed bilaterally (Fig. 3A). Under microscopy, many metastatic lesions with different sizes were observed to be distributed in bilateral sides of lung. The largest lesion located at the right lower lobe was 0.5 mm in diameter, corresponding to the right side tumor signal and the second largest lesion located at the left upper lobe was 0.3 mm in diameter, corresponding to the left side tumor signal in whole animal imaging (Fig. 3C). In another mouse, a single tumor signal was detected and pathological examination revealed a tumor mass of 0.6 mm in diameter located near the left pulmonary hilus (Fig. 3B). Multiple microscopic metastatic lesions were also observed in the third mouse with very weak tumor signals.

Discussion

Luciferase has served as a reporter in a number of targeted gene expression experiments over the last two decades (1,2). In recent years, luciferase-based BLI is becoming an important and rapidly advancing field to visualize and quantify the proliferation of tumor cells in animal models (10-11). Luciferase-labeling is superior to other reporters such as GFP for tracing the progression of neoplastic growth from a few cells to extensive metastasis (12, 13). In spite of the remarkable progress made, much more remains to be done with luciferase visualization of tumors in vivo. In the present study, we established three animal models of human breast cancer using stably luciferase-transfected cells. Regardless of the tumor sites in subcutaneous tissue or in mammary gland fat pad, the tumors could be clearly imaged with extremely low background by whole animal imaging. Interestingly, the dynamics of the tumor signal intensity was significantly different among tumors. Some tumors quickly reached the maximal intensity. The time to reach the maximal signal was independent of tumor volume and was also not related to the maximal tumor signal. Apparently, there were individual differences in light emission following administration of luciferase. The tumor heterogeneity with respect to size, vascular density, blood supply and other factors may affect accessibility and retention of luciferase and consequently the kinetics of light emission. However, the maximal signal intensity is largely dependent on ATP levels in the tumor and the tumor volume. Bioluminescent signal could be used as an indicator of tumor biomass. One issue of concern is the selection of time point to measure the signal

intensity following luciferin administration. In the previous studies, the bioluminescent signal at 5 min time point was arbitrarily used to represent the tumor in various analyses (4, 5). Based on our dynamic analysis, it was clear that the signal at 5 min time point less precisely reflected the real signal intensity of a given tumor. The maximal signal at peak time point may be more reliable because of the significant correlation between the maximal signal and tumor volume. Of course, it is time- and labor-consuming to determine the maximal intensity individually.

One potential use of BLI is detection of metastasis in animals. The whole animals can be monitored through whole animal imaging. Wetterwald et al showed by using a bone metastasis model that micro-metastasis of 0.5 mm^3 volume can be detected, which reveals greater sensitivity than radiographic methods (14). A study by Edinger et al using luciferase-expressing HeLa cells demonstrated that 1 x 10^3 cells in the peritoneal cavity, 1 x 10^4 cells at subcutaneous sites and 1 x 10^6 circulating cells could be observed immediately postinjection of the cells (15). In the present study, clear signal from metastatic lesions could be detected when pulmonary metastatic lesions approached 0.3 mm in diameter. The lesions at this stage were still difficult to be differentiated from the vessel spots in MRI (data not shown). All of these studies using different models confirmed the high detection sensitivity of metastatic lesions using BLI. To date, the conventional methods used to test the effect of novel therapies on primary tumors and metastasis in vivo are time- and labor-consuming. The characteristics of luciferase-based BLI such as high sensitivity, real time, non-invasiveness and significant correlation of the signal with tumor growth markedly simplify such kinds of in vivo analysis that rely on animals (16). The therapeutic efficacy of a drug can be assessed without having to sacrifice the mice to search for tumor growth at primary and metastatic sites. Statistically significant results can be achieved by using a small number of mice since multiple measurements can be made over time. A major disadvantage of BLI is the difficulty in quantification of multiple micro-metastatic lesions and comparative analysis among lesions in different sites of the body is impossible due to the photon characteristics and tissue difference in photon pathways.

Acknowledgement:

This work was supported in part by DoD USAMRMC W81XWH-05-1-0291 and DAMD 17- 03-1-0759, DAMD 17-03-1-0123, NIH 5U54CA091431 and grant 2G12 RR003048 from the RCMI Program, Division of Research Infrastructure, National Center for Research Resources, NIH.

References

1. Massoud TF, Gambhir SS. Molecular imaging in living subjects: seeing fundamental biological processes in a new light. *Genes Development* 2003; 17:545-580.
2. Greer III LF, Szalay AA. Imaging of light emission from the expression of luciferases in living cells and organisms: a review. *Luminescence* 2002; 17:43-74.
3. Yu YA, Shabahang S, Timiryasova TM et al. Visualization of tumors and metastases in live animals with bacteria and vaccinia virus encoding light-emitting proteins. *Nat Biotech*. 2003; 22:313-320.
4. Jenkins DE, Hornig YS, Oei Y, Dusich J, Purchio T. Bioluminescent human breast cancer cell lines that permit rapid and sensitive in vivo detection of mammary tumors and multiple metastases in immune deficient mice. *Breast Cancer Res* 2005; 7:R444-R454
5. Nogawa M, Yuasa T, Kimura S et al. Monitoring luciferase-labeled cancer cell growth and metastatsis in different in vivo models. *Cancer Lett*. 2005; 217:243-253.
6. Sarraf-Yazdi S, Mi J, Dewhirst MW, Clary BM. Use of in vivo bioluminescence imaging to predict hepatic tumor burden in mice. *J Surg Res*. 2004; 120:249-255.
7. Zhang W, Moorthy B, Chen M et al. A Cyp1a2-luciferase transgenic CD-1 mouse model: responses to aryl hydrocarbons similar to the humanized AhR mice. *Toxicol Science* 2004; 82:297-307.
8. Pillon A, Servant N, Vignon F, Balaguer P, Nicolas JC. In vivo bioluminescent imaging to evaluate estrogenic activities of endocrine disrupters. *Analyt Biochem*. 2005; 340:295-302.
9. Vooijs M, Jonkers J, Lyons S, Berns A. Noninvasive imaging of spontaneous retinoblastoma pathway-dependent tumors in mice. *Cancer Res*. 2002; 62:1862-1867.
10. Ghosh M, Gambhir SS, De A, Nowels K, Goris M, Wapnir I. Bioluminescent monitoring of NIS-mediated (131)I ablative effects in MCF-xenografts. *Mol Imaging* 2006; 5:76-84.
11. Paulmurugan R, Massoud TF, Huang J, Gambhir SS. Molecular Imaging of drug-modulated protein-protein interactions in living subjects. *Cancer Res*. 2004; 64:2113-2119.
12. Choy G, O'Connor S, Diehn FE et al. Comparison of noninvasive fluorescent and bioluminescent small animal optical imaging. *Biotechniques* 2003; 35:1022-1026.
13. Troy T, Jekic-McMullen D, Sambucetti L, Rice B. Quantitative comparison of the sensitivity of detection of fluorescent and bioluminescent reporters in animal models. *Mol Imaging* 2004; 3:9-23.
14. Wetterwald A, van der Pluijm G, Sijmons B et al. Optical imaging of cancer metastasis to bone marrow: a mouse model of minimal residual disease. *Am J Pathol*. 2002; 160:1143-1153.

15. Edinger M, Sweeney TJ, Tucker AA, Olomu AB, Negrin RS, Contag CH. Noninvasive assessment of tumor cell proliferation in animal models. *Neoplasia* 1999; 1:303-310.
16. Hardy J, Edinger M, Bachmann MH, Negrin RS, Fathman CG, Contag CH. Bioluminescence imaging of lymphocyte trafficking in vivo. *Exp Hematol*. 2001; 29:1353-1360.

Figure Legends

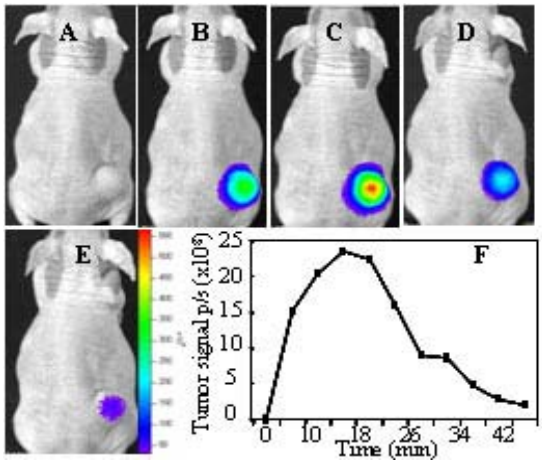

Fig. 1. Dynamic change of the bioluminescent signal in tumors following administration of D-luciferin, showing gradual increase and then decrease over time. Panels A to E represent the whole animal images taken separately at 0, 10, 15, 30 and 40 min after luciferin administration. Panel F shows the plot of signal intensity from tumor as a function of time after injection of luciferin.

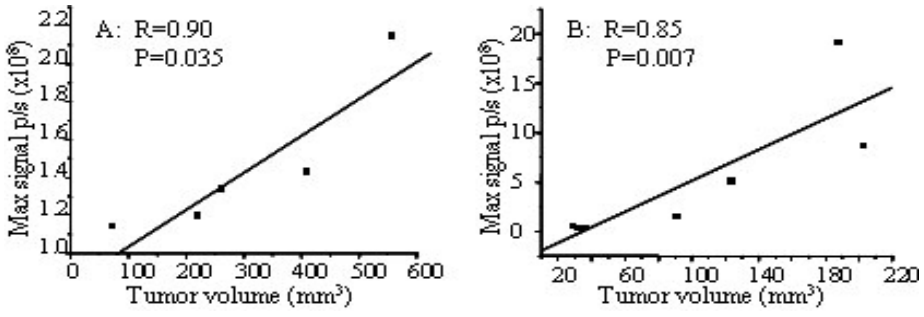

Fig. 2. Close correlation between maximal signal of tumors and tumor volume. A: solid tumor xenografts in the mammary gland fat pads of mice. B: subcutaneous tumors in the backs of mice.

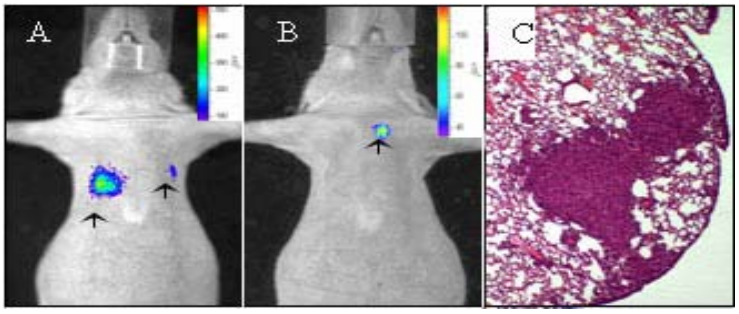

Fig. 3. Detection of lung metastasis through whole animal imaging. Panel A is the image from one mouse showing signals in bilateral sides of the lung. Panel B is the image from a mouse with signal from one tumor in the left upper lobe of the lung. Panel C represents the pathological finding of the left tumor in panel A (HE stain, x 40).

JrnlID 10278_ArtID 9019_Proof# 1 - 10/02/2007

Journal of Digital Imaging

A Mammography Database and View System for African-American Patients

Shani Ross,[1] O'tega Ejofodomi,[2] Ahmed Jendoubi,[2] Lisa Kinnard,[3] Mohamed Chouika,[2] Ben Lo,[3] Paul Wang,[2] and Jianchao Zeng[2]

We have digitized mammography films of African-American patients treated in the Howard University Hospital Radiology Department and have developed a database using these images. Two hundred and sixty cases totaling more than 5,000 images have been scanned with a high resolution Kodak LS85 laser scanner. The database system and web-based search engine was developed using MySQL and PHP. The database has been evaluated by medical professionals, and the experimental results obtained so far, are promising with high image quality and fast access time. We have also developed an image viewing system, D-Viewer, to display these digitized mammograms. This viewer is coded in Microsoft Visual C# and is intended to help medical professionals view and retrieve large data sets in near real time. Finally, we are currently developing an image content-based retrieval function for the database system to provide improved search capability for the medical professionals.

KEY WORDS: African-American women, breast cancer, database, mammography, mammogram, digitization, image viewer, Howard university

INTRODUCTION

The American Cancer Society estimates that in the United States alone, approximately 40,000 women die each year from breast cancer and that over 200,000 new breast cancer cases are diagnosed each year.[1,2] Typically, there are four main types of breast cancer: ductal carcinoma in situ (DCIS) where the cancer is confined within the ducts of the breast, lobular carcinoma in situ (LCIS) where the cancer is confined within the lobules or glands of the breast, invasive ductal carcinoma (IDC), and invasive lobular carcinoma (ILC).[1,3] IDC and ILC refer to the type of breast cancer where the tumor has spread from the ducts or lobules it originated from, respectively, into the surrounding tissue of the breast. Other less common breast cancers include medullary carcinoma, mucinous carcinoma, Paget's disease of the nipple, Phyllodes Tumor, and tubular carcinoma.[3]

Breast cancer is grouped into stages which indicate the invasiveness of the disease. There are four stages—I, II, III, IV—defined by the American Joint Committee on Cancer[1,3] based on a combination of tumor size, lymph node involvement, and presence or absence of distant metastasis. There is also a more general classification: early/local stage where tumor is confined to the breast, late/regional stage where cancer has spread to the surrounding tissue or nearby lymph nodes, and advanced/distant stage where cancer has spread to other organs beside the breast.[1,4]

There has been a decline in breast cancer mortality rates of about 2.3% over the last decade[1,2] due to improved screening techniques leading to earlier detection, increased awareness,

[1]*From the Neural Engineering Lab, University of Michigan, 300 North Ingalls Building, room 900F, Ann Arbor, MI 48109, USA.*

[2]*From the Electrical Engineering, Howard University, Washington, DC, USA.*

[3]*From the Radiology, Georgetown University, Washington, DC, USA.*

Correspondence to: Shani Ross, Neural Engineering Lab, University of Michigan, 300 North Ingalls Building, room 900F, Ann Arbor, MI 48109, USA; tel: +1-734-9367699; fax: +1-734-9362116; e-mail: shross@umich.edu

doi: 10.1007/s10278-007-9019-6

and improved treatments. Improved screening techniques include regular self breast examination, breast physical examination by a doctor, and regular mammogram examinations. In a mammogram, a radiologist looks for any unusual signs. These include asymmetry between the two breasts, any irregular areas of increased density, or any areas of skin thickening all of which can indicate whether there is a mass, or lump, in the breast tissue.[1,3] As this mass can either be cancerous or benign, further tests such as a biopsy of the suspicious area are done to differentiate between the two. In addition, doctors look for calcifications which are tiny calcium deposits that indicate changes within the breast possibly pointing to cancer. Microcalcifications especially are usually associated with cancer.

Despite improved screening techniques, this decline has been much smaller in African-American women compared to Caucasian-American women even with increased participation by African-Americans in routine mammography screening since 1980.[5] Furthermore, statistics have shown that although Caucasian-American women have an overall higher incident rate of breast cancer than African-American women, African-American women have a slighter higher incident rate of breast cancer before the age of 35 and are more likely to die of breast cancer at any age.[1,6] Also, in comparison to Caucasian women, African-American women are less likely to be diagnosed with tumors of diameter less than or equal to 2.0 cm and in the early stage of breast cancer, but more likely to be diagnosed with tumors of diameters greater than 2.0 cm and in later and advanced stages of the cancer.[1,6,7] Some of this disparity could be explained by an overall lower socioeconomic status, unequal access to medical care, and additional illnesses,[8–10] which results in a much smaller percentage of African-American women getting early and regular mammograms compared to Caucasian women. Hence, they are usually not diagnosed with cancer until at a much later date when the cancer is at an advanced stage, which increases their mortality risk.

Some studies have also reported differences in breast cancer histology in African-American women and Caucasian women, although they noted that these results are not conclusive. Some of these studies found that African-American women had a greater chance of developing ductal tumors, whereas Caucasian women had a greater chance of developing more lobular tumors.[11,12] This could be significant in the difference in outlook for the two racial groups, as lobular carcinoma is usually less aggressive. Other studies reported that African-American women had a greater frequency of medullar carcinoma than Caucasian women.[5,7] Medullary carcinoma is similar to ductal carcinoma but has a clearer distinction between the cancerous and normal cells.

Perhaps the most statistically significant differences seen between the two racial groups are the steroid receptor status of the tumor and the tumor proliferation rates. These differences are evident even when comparisons were adjusted for age, stage, treatment and screening opportunities, and risk factors. Typically African-American women had more estrogen- and progesterone-receptor negative tumors. Such tumors are generally unaffected by changing levels of these hormones and are thus less responsive to antihormonal treatments. African-American women also tended to have more poorly defined tumors, increased cell growth, and marked tumor necrosis. All these factors contribute to more aggressive tumors for African-American women.[5,7,11,12]

The epidemiological and tumor biology differences seen in African-American women compared to Caucasian women, leading to higher mortality rates, stresses the particular importance in trying to fully understand why these disparities arise. One possible step towards addressing these issues is to have a larger number of African-American breast cancer cases available for study. Currently, there are no breast cancer databases primarily developed for African-American patients, although general breast cancer database systems do exist.[13,14] Hence, the main objective of this research is to develop the first major African-American Breast Cancer Mammography database for the use of training radiologists and other personnel involved in the detection and treatment of breast cancer. This could thus help in further understanding the nature of the breast cancer in African-American women. Part of this study also includes developing a view system that will allow radiologists to retrieve and view the digital imaging and communications (DICOM)-formatted images in the database in near real time.

This research is divided into three main parts. The first part is the collection of actual data for the

database, which includes the obtaining, scanning, and organization of the mammography films. The second part is the development of the database and web-search engine using database management software and webpage development programming languages. The third part is the development of the viewing software.

METHODS

This study is collaboration between the Howard University Electrical Engineering Department, the Howard University Hospital Radiology Department, and the Georgetown University Radiology Department. The database and viewing software development are being done through the Howard University Electrical Engineering Department with the films being supplied by the Howard University Hospital Radiology Department. Consulting support is provided by the Georgetown University Radiology Department. Before conducting the study, approval was obtained from the Institutional Review Board. The primary investigators, who worked directly with the films, took the Human Participants Protection Education for Research Teams online certification course[15] to meet the National Institute of Health (NIH) requirements on patient privacy issues. The investigators also attended seminars required by Howard University Hospital on the Health Insurance Portability and Accountability Act (HIPAA) of 1996.

Digitization of the Mammography Films

Film Collection

Currently, mammography films from 260 patients from the Howard University Radiology Department have been digitized and entered into the database. All of these patients were diagnosed with breast cancer between 1994 and 2004 and were between the ages of 24 and 88. The patients' histology includes masses of different sizes with and without poorly defined borders, microcalcifications, clusters of calcifications, adenopathy, heterogeneous density, and solid nodules. Furthermore, the majority of these patients had undergone more than one mammography examination. For these patients, the earlier exams typically were regular screening mammograms, which showed normal and benign images. Normal images were mammograms in which nothing suspicious was seen, and benign images were mammograms in which something suspicious was seen initially but with further examination found to nonmalignant. The cancer appeared and was diagnosed in the later exam dates. Thus, we were able to obtain a wide variety of films showing normal, benign, and cancerous images. Table 1 gives an overview of the patient characteristics of the database.

Each examination date, on average, contained four films corresponding to the four typical views taken of the breasts during a mammogram. These views are: left mediolateral oblique view (LMLO), right mediolateral oblique view (RMLO), left craniocaudal view (LCC), and right craniocaudal view (RCC) (Fig. 1). The films generally came in two sizes: 8×10 and 10×12 in.

Majority of these mammograms had been down at Howard University Hospital using the MGX 2000 mammography machine from Instrumentarium Corporation, Imaging Division, Tuusula, Finland. The machine parameters include: a film focus distance of 26 in., AGFA Mamoray HDR-C high dynamic range film 24 cm $\times$ 32 cm film type, exposure of 75–130 mAs (depends on patient), tube voltage of 27–30 KeV, and a filter of 0.025 mm molybdenum, or 0.025 mm rhodium, or 0.5 mm aluminum. Some of the older mammograms had been done at the patient's previous hospital and the technical parameters of the machine used are unknown.

Scanning and Technical Procedure

The scanner used is the Kodak LS85 Laser Digitizer, specifically designed for high resolution teleradiology. Films can be converted into high resolution digital images of up to 5,120 pixels by 6,140 lines with 12 bits per pixel. Each pixel is assigned an optical digital value equal to 1,000$\times$ optical density and has a spot size of 50 μm. The digitizer has a scan rate of approximately 75 lines per second. It was purchased along with accompanying support software from RADinfo Systems, Dulles, Virginia. This accompanying software supported the digitization and burning of the images and are: the Inter2000 Film Digitizer ™

Q2 t1.1 **Table 1. Representative Sample of the Patient Characteristics of the Database**

t1.2 Patient	Age	Year Cancer Diagnosed	Histology	Digitization Date
t1.3 MK833AI543	24	1999	Spiculated mass and speculated density in R. breast	6/10/2004
t1.4 WM980RI062	26	2001	Abnormal, dilated ducts and microcalcifications	6/14/2004
t1.5 BR815AA561	32	1999	Cluster of calcifications	1/22/2004
t1.6 TN989IA352	39	2001	Malignant calcifications in L. breast, extensive ductal carcinoma in situ	6/2/2004
t1.7 HS963AH074	45	1999	Large medial calcifications in L. breast	4/6/2004
t1.8 BM869OI885	46	1998	Microcalcifications in L. Breast	6/19/2004
t1.9 ME729OM197	55	2001	Malignant calcifications and solid mass	5/19/2004
t1.10 AJ337DU655	56	1997	Solid mass with poorly defined borders in L. breast	7/7/2004, 7/8/2004
t1.11 BJ567RA821	58	2001	Cluster of calcifications in L. Breast	1/30/2004
t1.12 GI759HZ353	59	1998	Microcalcifications and lateral calcifications in L. breast	6/21/2004
t1.13 DM795AA866	62	1999	Spiculated mass in R breast	3/25/2004
t1.14 BM169AE858	62	1996	Density with obscured borders in L. breast	6/20/2004
t1.15 MA935CN074	63	1999	Metastative adenopathy in L axillary	6/10/2004
t1.16 BD759AO805	65	2000	Breasts heterogeneously dense, highly suspicious mass with speculated borders and associated microcalcifications	2/24/2004, 3/1/2004
t1.17 SS913TY027	66	2000	R. breast ductal carcinoma in situ	6/1/2004
t1.18 DM710AA630	70	1998	Large mass and microcalcifications in R. breast	6/22/2004
t1.19 GN216OO404	70	1997	Macro and micro calcifications in R breast	6/22/2004
t1.20 KC717EL219	71	2000	R. breast carcinoma—irregular nodal density; Previous L. breast carcinoma (now irradiated)—spiculated mass with microcalcifications at the peripheral	5/28/2004
t1.21 CG362AE888	71	1998	Large pulp mass solid with lobulated borders, small satellite lesions and large abnormal axillary node in L. breast	6/21/2004
t1.22 BL316YO065	72	1999	Cluster of calcifications	1/23/2004
t1.23 DS833AA858	73	1997	Mass and poorly defined post border in R. breast	6/21/2004
t1.24 BM065RA569	74	1996	Malignant appearing calcifications in R. breast	6/19/2004
t1.25 FD103LE602	76	1998	Irregular asymmetric density with associated microcalcifications in L breast	7/15/2004
t1.26 JF393AR669	77	2001	Two spiculated masses, poorly defined	5/28/2004
t1.27 MD782IE169	82	1998	Spiculated mass in L breast	6/24/2004
t1.28 HK862AA996	83	2000	Solid and irregular polyp mass	5/17/2004

263 (I2000FD), RSVS Viewer ™, and CD Power-
264 PACS ™.
265 The I2000FD™ is the interface for the film
266 digitizer. This is where patient information is
267 entered, the digitizer is accessed for scanning,
268 and where any necessary changes can be made
269 to the film before the digital image is saved.
270 Before scanning, patient information required by

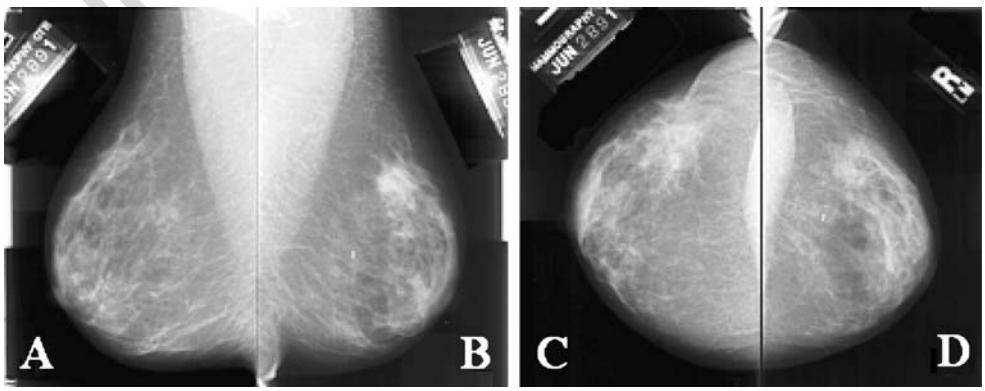

Fig 1. A typical mammography view: a LMLO, b RMLO, c LCC, and d RCC[13]

I2000FD™ is entered. This information includes: the patient name written in a code to preserve patient's privacy rights, birth date, exam date, the ascension number used to keep track of each series, and the time and date of digitization of each film. This information was the essential information required by the program to stamp and classify each resulting digitized image. Next, the user specifies the resolution, bit depth, window level settings, and size of the film to be scanned. In this study, films are digitized at a resolution of 512 pixels/in. and a bit depth of 12, both of which are maximum values of the scanner, to give the highest image quality. The scan size chosen is either 8×10 or 10×12 in., depending on the size of the film to be scanned. Once the settings have been entered, the film is loaded into the Kodak scanner and digitized. Furthermore, the software allows us to cover the patient's name and other identifying information so that this is not seen in the digitized image in the software. The images are then saved and copies of them are transferred to the viewing software (RSVS ™) and burning software (CD PowerPACS ™). The sizes of these saved images are generally 40 Mb for the 8×10 films and 60 Mb for the 10×12 films. The RSVS™ is a viewing software for DICOM-formatted images, which allow us to further view and verify the digitized images. The CD PowerPACS™ software allows us to save and transfer the images to CD-R storage media. This program also saves a copy of the RSVS viewer on each CD.

Development of the Database

The Howard University Mammography Database[16] was developed using PHP and MySQL. MySQL is a simple relational database management system that allows users to add, access, and process data stored in a database.[17] The database contains relevant information such as encrypted patient name, patient ID, date of birth, type of scanner used, number of series in a case, exam date, total image count in a case, malignancy, and available image views (RMLO, LCC, etc.). New information can also be added when necessary. Our database is linked to a web-based search engine powered by PHP-recursive acronym for "PHP: Hypertext Preprocessor,[18] which is a general-purpose open source scripting language that can be embedded in hypertext markup language (HTML for web-page development) and which can run directly on the server, unlike other languages such as java script. Queries on the database are carried out using PHP. In addition, digitized images and patient information are stored in the database using PHP. Information in the database is first entered into Microsoft EXCEL, and then from there, is imported into the MySQL tables via PHP. This process makes entering new information into the database less tedious than directly entering it into MySQL from the Microsoft Windows command line. Furthermore, a login web page for the web-based search engine is also developed using PHP to limit use of this system to authorized users only. After being logged on to the system, a user can then specify search criteria via the web page. The query is then searched through the MySQL database, and the search results are displayed on the web page. The results are displayed as a list of case names with links to the actual images.

Development of the D-Viewer

The D-viewer is a viewing system developed for visualizing the digitized mammograms. By using this system, radiologists would not only be able to perform various image manipulations, such as circling the area of the cancer and making notes on the image, but could also save these markings as needed. The view system uses graphical user interface (GUI) for easy use and is to be DICOM compliant. The D-viewer system is developed with Microsoft Visual C#, an object-oriented programming language from Microsoft that is easy for manipulating graphics and creating window forms. Currently, the system accepts the following image formats: Windows bitmap (bmp), joint photographic experts group (jpg), tagged image file format (tif/tiff), graphics interchange format (gif), and portable network graphics (png).

RESULTS

Mammography films from 260 patients, each having approximately 20 to 40 images, have been digitized using the Kodak LS85 Laser Scanner. This has resulted in over 5,000 digitized images that have been stored into our database. Many patients had typically 20 to 40 images because they did several

regular screening mammograms before the mammography exam in which the cancer was diagnosed. Hence, on average for each patient, one could be looking at 4–10 different exam dates each of which would contain the four films representing the four typical views (LMLO, RMLO, LCC, RCC). Sometimes, for a particular examination, extra images were taken, depending on if the radiologist was interested in a particular region. All these patients are African-American women from Howard University Hospital who have been diagnosed with cancer between the years 1994 and 2004. In addition, we can compare normal images and images of benign and malignant lesions of the same patient. The image quality is excellent, as the films were digitized at the highest resolution possible by the Digitizer, which was at 512 pixels per inch at a bit depth of 12. Furthermore, there were no observable distortions or artifacts due to the digitization process, although there is some concern that some noise may have been picked up due to possible dirt spots on the films. These images were also approved by the radiologist consultant associated with this study. The digitized image size is either 40 or 60 Mb, depending on the size of the mammogram film (8 × 10 or 10 × 12 in., respectively).

A database and a web-based search engine have been developed using MySQL and PHP. Patient information and the corresponding images can be retrieved when queries are made by selecting various criteria. A user is first required to login to access the database (Fig. 2). User accounts will be set up for general users just wanting to learn more about breast cancer and to peruse the database and for users requesting more functionality from the database, such as being able to download the images.

After a person logs in, they are directed to the web-search page where they can select their search criteria (Fig. 3). Currently, the search criteria available include whether the image is normal, benign, or cancer, the year the patient was born, the year the exam was done, total number of examinations for a patient, total number of images for a patient, and the mammography view. For example, a person may want to see all the cancer images of patients who were diagnosed with cancer during 1999–2000 and were born during 1961–1970. There is also a reset button on this page that clears all the search fields. After the search criteria has been selected and submitted, the database returns a list of all patient cases corresponding to that search. The list of cases contains the code name associated with that patient, each series and corresponding exam date of that series, the digitization date for each series, the total number of images in each series, and all available image views done. Figure 4 shows a sample results page of a search.

Finally, Figure 5 shows a snapshot of the D-viewer system with the LCC and RCC views of one of our digitized mammograms. The system can accept bitmap, tiff, jpeg, gif, and png image formats. The D-viewer is currently under development.

DISCUSSION

Our research attempts to provide the first major breast cancer database for African-American women. This would allow radiologists and other applicable parties to study various types of African-American women breast cancer cases. Howard University Hospital was chosen not only

Fig 2. Login page of the web-based search engine linked to the breast cancer database

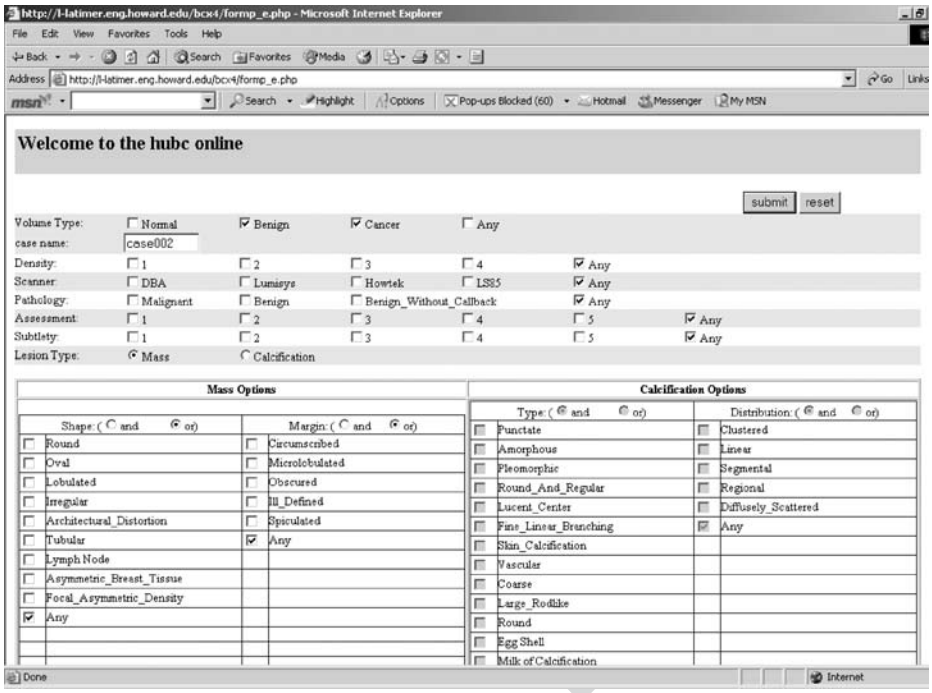

Fig 3. Web-based search page

for its accessibility, but more importantly, because it services a large African-American community in the Washington DC, Maryland, and Virginia area, thus, providing a large number of African-American women mammography cases. This research is also significant in an effort to close the gap of diversity in breast cancer mortality.

However, this research is not just about digitizing a large number of mammograms. The database is also being developed as an online

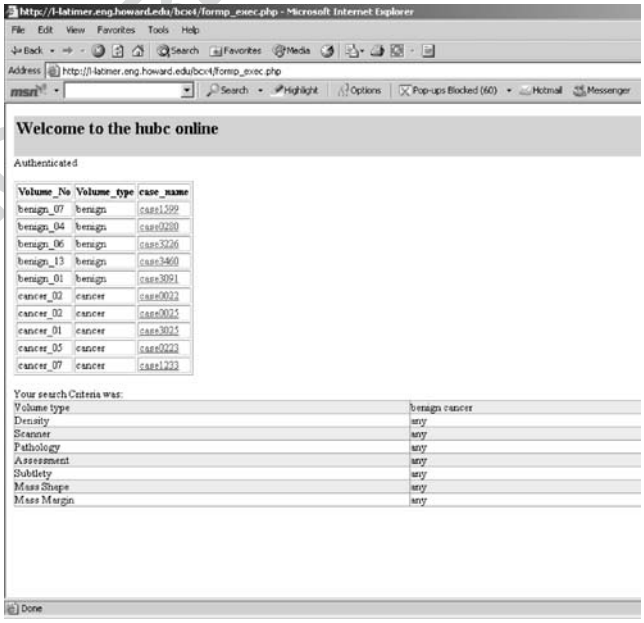

Fig 4. Results page of search

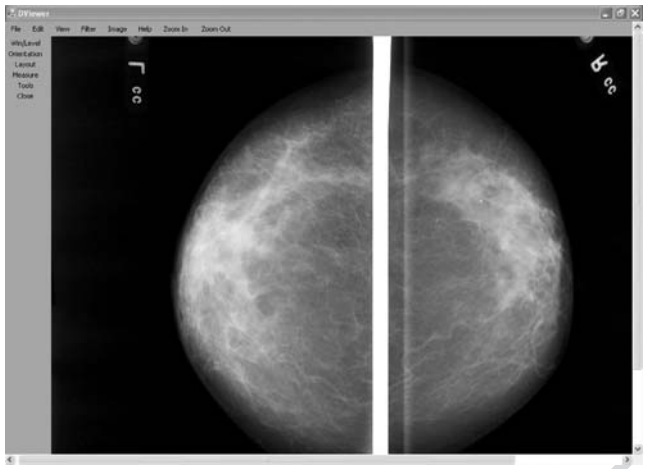

Fig 5. D-viewer user interface

interactive teaching/training tool geared towards both the radiology students and others interested in learning more about breast cancer. For example, the site would contain general information on breast cancer and more detailed information. Medical students could be asked to perform tasks such as determining, from the image alone, the search criteria required to produce that particular image. This would require the students to be able to accurately identify specific characteristics of that image. Radiologists could also use this database to help their diagnosis process of difficult new cases by searching for similar cases or images.

Our database differs from current major databases such as the one developed by the University of South Florida[14] in that our patient data set consists of African-American women only, unlike other databases which consist primarily of Caucasian patients. Furthermore, we intend our database to be an interactive training tool where the users can look at images and guess the search criteria that they would have had to put in to obtain that image. We also plan to extend the functionality of the database by making it an image-based retrieval system in which features in the image can be used to define the search criteria.

CONCLUSIONS

We have digitized more than 5,000 mammography images of 260 African-American women patients and developed a database and viewing system for these images. All patients in this study have already been diagnosed with breast cancer. The digitized images include normal, benign, and malignant mammograms, which were taken between the years 1994 and 2004. The normal and benign mammograms of a patient were from routine screenings done before breast cancer was diagnosed. All the mammography images are searchable in the database system via a web-based search engine. They can be viewed in the viewing system and easily manipulated during the viewing process.

Further research will be performed to improve the database and the viewing system. First of all, we will seek input from radiologists when they test our database and viewing system. They will be asked to identify key information from the images such as the presence or absence of malignant cancer, location of cancer, type of cancer (mass or calcification), assessment, subtlety, and density of the breast. Locations of the cancers, if present, on the digitized mammograms, will be marked and saved. The database will also be updated with these added data.

New mammograms will also be collected and digitized to increase the size of our database. The D-viewer system will be further enhanced to improve its functionalities based upon input from the radiologists after testing the system. We will also develop an interactive web-based learning/training/testing system, which can provide detailed information on breast cancer, training sessions for

breast cancer diagnosis, and test platforms. To improve the quality and versatility of our database, we plan to develop an image-based retrieval database, whereby, we can use images instead of words to determine our search criteria. For example, if we circle a region of interest on an image such as a mass, we could query the database to return all images and corresponding information that have a similar region of interest.

This database will be made accessible to radiologists and students via announcements on the Howard Medical School website and on the Howard University Electrical and Computer Engineering Department website. No fees will be charged for basic database access, but fees will be charged for any advanced functions such as image processing or content-based retrieval operations.

ACKNOWLEDGEMENTS

We would like to thank the radiologists and other medical professionals in the Department of Radiology at Howard University Hospital who made significant contributions to this research. This research was supported by the US Army Medical Research and Material Command under DAMD 17-01-1-0267, W81XWH-05-1-0291, and DAMA17-00-1-0291. This publication was also made possible, in part, by a grant Number 2G12RR003048 from the National Center for Research Resources (NCRR), a component of the NIH.

REFERENCES

1. American Cancer Society: Breast Cancer Facts and Figures 2005–2006. Atlanta, GA: American Cancer Society, Inc., 2005

2. American Cancer Society: Cancer Facts and Figures 2006. Atlanta, GA: American Cancer Society, Inc., 2006

3. Abeloff MD, Wolff AC, Wood WC, McCormick B, Weber BL: Cancer of the Breast. In: Clinical Oncology, Philadelphia, PA: Elsevier, 2004

4. Young Jr, JL, Roffers SD, Ries LAG, Fritz AG, Hurlbut A, Eds.: SEER Summary Staging Manual—2001: Codes and Coding Instructions, Bethesda, MD: National Cancer Institute, 2001

5. Rovak-Schaler R, Rose DP: Mammography screening and breast cancer biology in African American women—a review. Cancer Detec Prev 26:180–191, 2002

6. SEER Cancer Statistics Review, 1975-2002, National Cancer Institute. Available at http://seer.cancer.gov/csr/1975_2002/. Accessed 31 May 2006

7. Elledge RM, Clark GM, Chamness GC, Osborne CK: Tumor biologic factors and breast cancer prognosis among white, hispanic, and black women in the United States. J Natl Cancer Inst 86:705–712, 1994

8. Bach PB, Schrag D, Brawley OW, Galaznik A, Yakren S, Begg C: Survival of blacks and whites after a cancer diagnosis. JAMA 287:2106–2113, 2002

9. Josyln SA: Racial differences in treatment and survival from early stage breast carcinoma. Cancer 95:1759–1766, 2002

10. Shavers VI, Brown ML: Racial and ethnic disparities in the receipt of cancer treatment. J Natl Cancer Inst 95:334–357, 2002

11. Chlebowski RT, Chen Z, Anderson GL, Rohan T, Aragaki A, Lane D, Dolan N, Paskett E, McTiernan A, Hubbell FA, Adams-Campbell LL, Prentice R: Ethnicity and breast cancer factors influencing difference in incidence and outcome. J Natl Cancer Inst 97:439–448, 2005

12. Porter PL, Lund MJ, Lin MG, Yuan X, Liff JM, Flagg EW, Coates RJ, Eley JW: Racial differences in the expression of cell cycle-regulatory proteins in breast carcinoma: study of young African American and white women in Atlanta, Georgia. Cancer 100:2533–2542

13. Digital Database for Screening Mammography. Available at http://figment.csee.usf.edu/Mammography/DDSM/thumbnails/normals/normal_01/case0130/A-0130-1.html. Accessed 31 May 2006

14. University of South Florida Digital Mammography Home Page. Available at http://figment.csee.usf.edu/Mammography/Database.html. Accessed 31 May 2006

15. Human Participant Protections Education for Research Teams, National Cancer Institute. Available at http://cme.cancer.gov/clinicaltrials/learning/humanparticipant-protections.asp. Accessed 31 May 2006

16. Ross S, Ejofodomi O, Jendoubi A, Chouikha M, Lo B, Wang P, Zeng J: A mammography database and view system for the African American patients. In: Emerging Technologies and Applications for Imagery Pattern Recognition, Los Alamitos, CA: IEEE Computer Society, 2005

17. MySQL Reference Manual. Available at http://dev.mysql.com/doc/refman/5.0/en/. Accessed 31 May 2006

18. PHP: PHP Manual - Manual. Available at http://www.phpbuilder.com/manual/. Accessed 31 May 2006

AUTHOR QUERIES

AUTHOR PLEASE ANSWER ALL ALL QUERIES.

Q1. "Washington", "DC", and "USA" were captured as the city, state, and country, respectively. Please check if appropriate.
Q2. "polp" was changed to "polyp". Please check if appropriate.

Reversal to cisplatin sensitivity in recurrent human ovarian cancer cells by NCX-4016, a nitro derivative of aspirin

Anna Bratasz*, Nathan M. Weir*, Narasimham L. Parinandi*, Jay L. Zweier*, Rajagopalan Sridhar†, Louis J. Ignarro‡§, and Periannan Kuppusamy*¶

*Center for Biomedical Electron Paramagnetic Resonance Spectroscopy and Imaging, Comprehensive Cancer Center, The Dorothy M. Davis Heart and Lung Research Institute, Department of Internal Medicine, Ohio State University, Columbus, OH 43210; †Department of Radiation Oncology, Howard University Hospital, Washington, DC 20060; and ‡Department of Molecular and Medical Pharmacology, Center for the Health Sciences, University of California School of Medicine, Los Angeles, CA 90095

Contributed by Louis J. Ignarro, December 28, 2005

Ovarian cancer is a gynecological malignancy that is commonly treated by cytoreductive surgery followed by cisplatin treatment. However, the cisplatin treatment, although successful initially, is not effective in the treatment of the recurrent disease that invariably surfaces within a few months of the initial treatment. The refractory behavior is attributed to the increased levels of cellular thiols apparently caused by the cisplatin treatment. This observation prompted us to choose a cytotoxic drug whose activity is potentiated by cellular thiols with enhanced specificity toward the thiol-rich cisplatin-resistant cells. We used NCX-4016 [2-(acetyloxy) benzoic acid 3-(nitrooxymethyl)phenyl ester], a derivative of aspirin containing a nitro group that releases nitric oxide in a sustained fashion for several hours in cells and *in vivo*, and we studied its cytotoxic efficacy against human ovarian cancer cells (HOCCs). Cisplatin-sensitive and cisplatin-resistant (CR) HOCCs were treated with 100 μM NCX-4016 for 6 h, and/or 0.5 μg/ml cisplatin for 1 h and assayed for clonogenecity. NCX-4016 significantly reduced the surviving fractions of cisplatin-sensitive (63 ± 6%) and CR (70 ± 10%) HOCCs. NCX-4016 also caused a 50% reduction in the levels of cellular glutathione in CR HOCCs. Treatment of cells with NCX-4016 followed by cisplatin showed a significantly greater extent of toxicity when compared with treatment of cells with NCX-4016 or cisplatin alone. In conclusion, this study showed that NCX-4016 is a potential inhibitor of the proliferation of CR HOCCs and thus might specifically kill cisplatin-refractory cancer cells in patients with recurrent ovarian cancer.

cisplatin resistance | glutathione | nitric oxide | cytotoxicity | nonsteroidal antiinflammatory drug

Ovarian cancer is the second most commonly diagnosed gynecological malignancy and the fourth leading cause of mortality among women in the United States (1). The high mortality rate is attributed to the lack of early diagnosis of the malignancy and difficulties associated with treatment. The standard treatment includes cytoreductive surgery followed by the administration of chemotherapeutic agents. Platinum-based compounds (e.g., cisplatin and carboplatin) in combination with taxanes (e.g., taxol or paclitaxel), anthracyclines (e.g., doxorubicin), or alkylating agents (e.g., melphalan) are administered to treat the advanced-stage disease (2). However, the overall clinical response with such treatments is only 40–60%. The primary factor that limits the success of chemotherapy in ovarian cancer is the acquired drug resistance in the tumor cell population. Administration of cisplatin results in the development of drug resistance in the cancer cells. Postulated mechanisms of drug resistance include decreased intracellular accumulation of the drug, increased levels of thiols, which inactivate the platinum compound, and the enhancement of DNA repair (3). Even a slight increase in the cisplatin resistance of the tumor may pose a clinically important problem requiring administration of large doses of the drug, which may lead to severe multiorgan toxicities (4). Therefore, a new adjuvant treatment is necessary to specifically overcome the thiol-mediated drug resistance in the treatment of recurrent ovarian cancer.

Recently, Ignarro and coworkers (5, 6) showed that nitric oxide (NO) is capable of inhibiting the proliferation of rat aortic smooth muscle cells in a cGMP-independent pathway. The cytostatic action of NO was attributed to its inhibitory effect on ornithine decarboxylase, an enzyme that generates spermine, spermidine, and putrescine, which are required for cell proliferation. Earlier, Wink *et al.* (7) showed enhanced cytotoxicity of cisplatin in Chinese hamster V79 lung fibroblast cells pretreated with NO donors in a time-dependent manner. The enhancement of cisplatin cytotoxicity by pretreatment with diethylamine/NO (DEA/NO) and (propylamino)propylamine/NO (PAPA/NO) persisted up to ≈2 and 3 h, respectively, and thereafter the cytotoxicity of the drug returned to a level that was exhibited by the cisplatin treatment alone. In a more recent study by Riganti *et al.* (8), it was shown that NO reverted resistance to doxorubicin in a multidrug-resistant human epithelial colon cancer cell population by increasing the drug accumulation inside the cells in a cGMP-independent pathway. Thus, it appeared that NO-releasing drugs may have potential cytostatic effects on proliferating cells. However, it was not known whether the NO donors had a selective effect on cancer cells and what factors influenced the targeting of a particular cancer cell.

Cellular thiols have been shown to be involved in the mechanism of action of certain NO donor molecules. For example, it was reported that NO donors such as glyceryl trinitrate (GTN) and sodium nitroprusside induced cytotoxicity and mutations in Mutatect cancer cell lines and that the extent of mutagenecity was dependent on the cellular glutathione (GSH) levels (9). Chen *et al.* (10) identified the enzymatic bioactivation of GTN in mouse macrophage RAW cells mediated by mitochondrial aldehyde dehydrogenase that generates nitrite and, subsequently, NO. It has been suggested that thiols (2-mercaptoethanol or DTT) were required for this conversion. These observations prompted us to hypothesize that the thiol-rich environment in cisplatin-resistant (CR) ovarian cancer cells may potentiate NO production from a similar nitrate-based drug and may exert

Conflict of interest statement: No conflicts declared.

Abbreviations: GSH, glutathione; CR, cisplatin-resistant; CS, cisplatin-sensitive; HOCC, human ovarian cancer cell; MGD, *N*-methyl-D-glucamine dithiocarbamate; SNAP, *S*-nitroso-*N*-acetyl-penicillamine; SIN-1, 3-morpholinosydnonimine; NSAID, nonsteroidal antiinflammatory drug.

§To whom correspondence may be addressed. E-mail: lignarro@mednet.ucla.edu.

¶To whom correspondence may be addressed at: The Dorothy M. Davis Heart and Lung Research Institute, Ohio State University, 420 West 12th Avenue, Room 114, Columbus, OH 43210. E-mail: kuppusamy.1@osu.edu

 www.pnas.org/cgi/doi/10.1073/pnas.0511250103

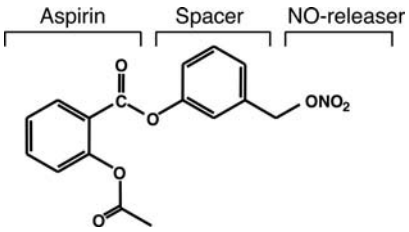

Fig. 1. Molecular structure of NCX-4016. The nitroaspirin consists of acetylsalicylate (aspirin, ASA) linked to a spacer moiety by an ester bond. An NO-releasing moiety ($-ONO_2$) is attached to the spacer. The drug is metabolized in cells by esterases to yield the parent drug (aspirin) and the spacer attached to the NO-releasing moiety, which is subsequently metabolized to release NO.

preferential cytostatic effect. The elevated levels of thiols in the CR cells presumably may increase the production of NO from a donor drug and potentiate the tumoricidal efficacy of cisplatin.

The aim of the present work was to test the potency of a novel NO-releasing compound, NCX-4016 [2-(acetyloxy)benzoic acid 3-(nitrooxymethyl) phenyl ester] (Fig. 1), in inducing cytotoxicity in human ovarian cancer cells (HOCCs) with a particular emphasis on CR cells. NCX-4016, a nitro derivative of aspirin (nitroaspirin), had been shown to generate NO in human umbilical vein endothelial cells (11). Our hypothesis was that the sustained release of NO by nitroaspirin in the thiol-rich ovarian cancer cells would decrease cell survival and proliferation. We further hypothesized that the cytotoxicity of NCX-4016 might augment the effect of cisplatin by decreasing the thiol content in the cells. We tested our hypothesis by performing cell-survival (clonogenic) assays on cisplatin-sensitive (CS) and CR HOCCs treated with NCX-4016 and cisplatin. The results showed that NCX-4016 was a potent inhibitor of proliferation of ovarian cancer cells and further suggested that this drug can be used in combination with cisplatin for treatment of advanced human ovarian cancer.

Results

Effect of Cisplatin on the Clonogenecity of CS and CR Cells. The integrity of the CS and CR ovarian cancer cell lines, as well as their IC_{50} dose of cisplatin, were established by determining the effect of cisplatin on the colony-forming ability of the cells. Cells were treated with varying doses of cisplatin (0–30 μg/ml) for 1 h, and clonogenic assays were performed as described in *Materials and Methods*. Fig. 2 shows the surviving fractions of CS and CR cells as a function of cisplatin dose. The surviving fraction of CS cells was markedly reduced by cisplatin even at a low dose of the drug (for example, 8 $\pm$ 2% survival at 1 μg/ml). The proliferation of the CS cells was almost completely inhibited by cisplatin at a dose of 5 μg/ml. The IC_{50} dose of cisplatin for the CS cells was 0.6 μg/ml. On the other hand, cisplatin exerted lower cytotoxicity on CR cells. The observed IC_{50} dose of cisplatin for the CR cells, 16 μg/ml, was $\approx$25 times higher than that for the CS cells. The results clearly established that the CR cells were resistant to cisplatin treatment and that the CS cells were sensitive to cisplatin treatment.

Measurement of NO Generation in NCX-4016-Treated Cells. Although NCX-4016 has been shown to generate NO in human umbilical vein endothelial cells (11), it was not known whether it was capable of generating NO in HOCCs. We used EPR spectroscopy to detect the generation of NO in HOCCs treated with NCX-4016. CR cells (2×10^7 cells per milliliter) were incubated with 500 μM NCX-4016, and EPR measurements were performed by adding a solution of iron-*N*-methyl-D-glucamine dithiocarbamate (Fe-MGD), a water-soluble NO trap that forms

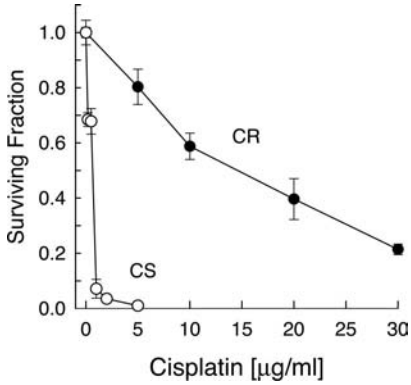

Fig. 2. Effect of cisplatin on the clonogenecity (surviving fraction) of HOCCs. CS and CR cells were incubated with various doses of cisplatin for 1 h, rinsed, and then plated in triplicate. The colony-forming assay was performed after 7 days. Data represent mean $\pm$ SEM obtained from 5–12 independent experiments and normalized to the value of the control cells. The cytotoxicity of cisplatin to CS cells was markedly greater (IC_{50} of 0.6 μg/ml) compared with that of CR cells (IC_{50} of 16 μg/ml).

a stable EPR-detectable paramagnetic complex, $Fe(MGD)_2$-NO. After 25 min of incubation of cells with NCX-4016, a characteristic triplet spectrum was observed, which continued to increase up to 90 min (Fig. 3). NCX-4016 alone or cells without NCX-4016 treatment did not show the characteristic NO spectrum upon treatment with Fe-MGD. The authenticity of the triplet EPR spectrum was established by measuring the EPR spectrum in a freshly mixed solution containing Fe-MGD and *S*-nitroso-*N*-acetylpenicillamine (SNAP), an NO-donor (Fig. 3). The triplet spectrum observed in the cells treated with NCX-4016 was identical to that observed in the SNAP control. Thus, the EPR data showed that NO was generated by NCX-4016 in HOCCs.

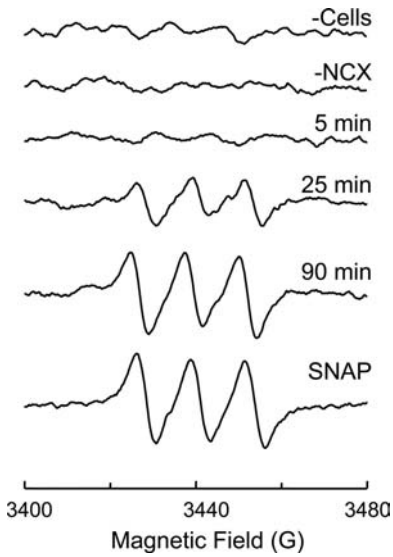

Fig. 3. EPR detection of NO generation by NCX-4016 in CR HOCCs. The CR cells were incubated with 500 μM NCX-4016 and $Fe(MGD)_2$, an NO spin trap for EPR detection; then the EPR spectrum was measured as a function of incubation time. A triplet spectrum with a splitting of 13.0 G was observed at 25 min and continued to grow with time up to 90 min. The authenticity of the spectrum was verified by comparing it with a spectrum measured under identical conditions and using SNAP, a known NO donor. The data showed that NO was released in the cells treated with NCX-4016.

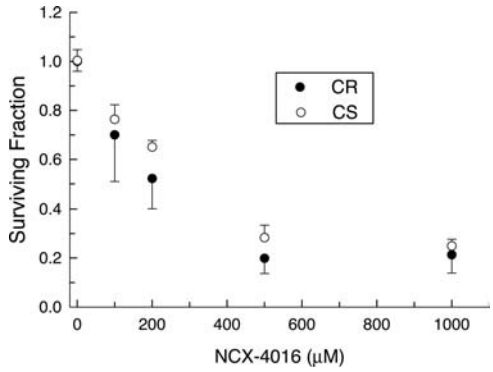

Fig. 4. Dose-dependent effect of NCX-4016 on the clonogenecity of HOCCs. CS and CR cells were incubated with different concentrations of NCX-4016 for 6 h, rinsed, plated in triplicate, and assayed for their clonogenecity after 7 days. Data represent mean ± SEM obtained from 4–10 independent experiments and normalized to the value of the corresponding control cells. The data showed that NCX-4016 exhibited a dose-dependent cytotoxicity in both the CS and CR cells.

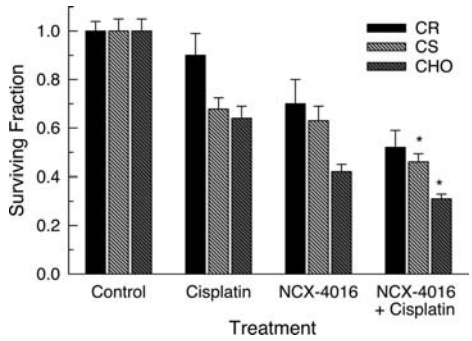

Fig. 6. Effect of NCX-4016 and cisplatin on the clonogenecity of HOCCs. CS, CR, or CHO cells were incubated with cisplatin (0.5 μg/ml) for 1 h, NCX-4016 (100 μM) for 6 h, or NCX-4016 followed by cisplatin, rinsed, plated in triplicate, and assayed for their clonogenecity after 7 days. Data represent mean ± SEM obtained from 3–12 independent experiments and normalized to the value of the corresponding control cells. *, $P < 0.001$ compared with the cisplatin-treated group. NCX-4016 exhibited markedly higher cytotoxicity in both the CS and CR cells.

Effect of NCX-4016 on the Clonogenecity of HOCCs. To assess the effect of NCX-4016 on the proliferation of HOCCs, clonogenic cell-survival assays on CR and CS cells treated with NCX-4016 were performed. Fig. 4 shows the surviving fractions of the CS and CR cells as a function of NCX-4016 dose at 6 h of drug incubation followed by 7 days in culture. The surviving fractions of both the CS and CR cells were significantly ($P < 0.001$) reduced by NCX-4016 in a dose-dependent fashion. Although the cytotoxic effect of NCX-4016 was consistently greater on CR cells compared with that on CS cells, the difference was not statistically significant.

We also studied the effect of exposure time of cells to NCX-4016 on the surviving fraction of cells. The cells were incubated for 1 or 6 h with 100 μM NCX-4016, and their surviving fractions were evaluated after 7 days in culture. It was observed that NCX-4016 treatment for 1 h did not show any significant effect compared with the control (data not shown). However, the same treatment for 6 h showed ≈30% reduction in the number of surviving colonies of both CS and CR cells.

To check whether the cytotoxicity of NCX-4016 was caused by the aspirin that arises from the metabolic cleavage of NCX-4016 in cells, we performed the clonogenecity assay in the presence of 100 μM aspirin and found that aspirin alone did not cause significant cytotoxic effect (Fig. 5). This suggested that cytotoxicity depended on the nitrate moiety of the drug.

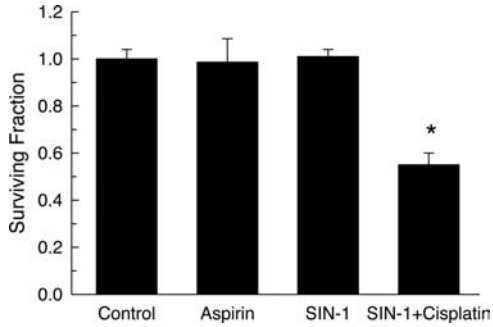

Fig. 5. Effect of aspirin, SIN-1, and SIN-1 with cisplatin on the clonogenecity of HOCCs. CR cells were incubated for 1 h with 100 μM aspirin, 100 μM SIN-1, or 100 μM SIN-1 with 0.5 μg/ml cisplatin, rinsed, plated in triplicate, and assayed for their clonogenecity after 7 days. Data represent mean ± SEM obtained from 3–10 independent experiments and normalized to the value of the corresponding control cells. *, $P < 0.001$ compared with controls.

We also verified whether the cytotoxic effect of NCX-4016 was due to its slow NO-releasing ability in cells. We performed additional experiments with 3-morpholinosydnonimine (SIN-1), which released NO in a relatively short time (≈10 min), in aqueous solutions, under physiological conditions (12). Treatment of the CR cells with 100 μM SIN-1 did not alter the surviving fraction (Fig. 5), suggesting that, at least in the case of CR cells, long-term exposure to NO was required for the observed cytotoxic effect.

Effect of NCX-4016 on the Cytotoxicity of Cisplatin. We further investigated the effect of NCX-4016 on cisplatin-induced cytotoxicity to HOCCs. CR and CS cells were treated with 100 μM NCX-4016 for 6 h, followed by 0.5 μg/ml cisplatin for 1 h, and then were assayed after 7 days of treatment. Fig. 6 shows the surviving fractions of cells treated with cisplatin and/or NCX-4016. The results showed that cisplatin was ineffective in CR cells (90 ± 9% surviving fraction) but caused a significant reduction in the number of colonies in CS cells (68 ± 5%). However, NCX-4016 significantly reduced the number of colonies in both CR (70 ± 10%) and CS (63 ± 6%) cells. On the other hand, treatment of cells with NCX-4016 followed by cisplatin treatment caused significantly higher cell killing (CR cells, 52 ± 7%; CS cells, 46 ± 3%) compared with cisplatin or NCX-4016 treatment alone.

We further evaluated the effect of cisplatin and NCX-4016 on the proliferation of a noncancer cell line, namely, Chinese hamster ovary (CHO) cells. The CHO cells were treated with NCX-4016 (100 μM) and/or cisplatin (0.5 μg/ml) as described above. The results showed significantly better cell-killing ability of the drugs in CHO cells compared with CR or CS cells. For example, the combination treatment in CHO cells showed 31 ± 2% survival compared with CS cells, which showed 46 ± 3% survival.

We further investigated whether the cellular concentration of NO during the pretreatment period was important in the potentiation of cisplatin-induced cytotoxicity and performed additional experiments with SIN-1. CR cells treated with SIN-1 (100 μM) for 1 h followed by 0.5 μg/ml cisplatin for 1 h showed survival of 55 ± 5%, which was significantly different from the survival of cells treated with SIN-1 alone (101 ± 3%) (Fig. 5). These results suggested that pretreatment of CR cells with NO potentiated the efficacy of cisplatin in overcoming the acquired drug resistance. The mode of NO generation, however, apparently was not critical for the regained cytotoxic effect of cisplatin.

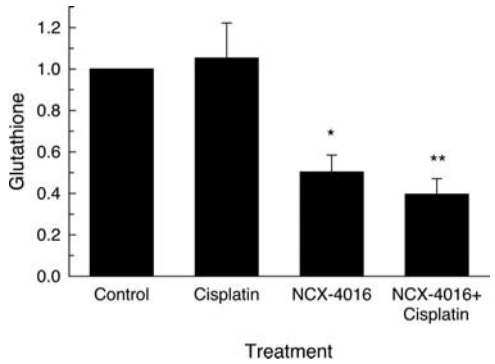

Fig. 7. Intracellular GSH levels in the CR cell lines treated with cisplatin and/or NCX-4016. The assays were performed by using EPR spectroscopy with a thiol-sensitive probe. *, $P < 0.01$ compared with control; **, $P < 0.01$ compared with control or cisplatin-treated group; not significant compared with NCX-4016-treated group. The CR cells treated with NCX-4016 show markedly lower levels of GSH compared with those treated with cisplatin.

Thiol Levels in CS and CR Cells. The cell proliferation assays described above suggested that the NCX-4016 alone was equally cytotoxic to both CS and CR cells and that the cytotoxic efficacy apparently did not depend on the nature of cisplatin sensitivity among cells. This observation was in striking contrast to the results obtained with cisplatin, whose cytotoxic efficacy showed a strong dependence on the nature of cisplatin sensitivity of the cell. Because it was established that cisplatin resistance in HOCCs was primarily governed by elevated levels of GSH, we further determined the thiol content of these cells. The CR cells that we used had 75 ± 10% higher levels of GSH compared with those of CS cells (data not shown). Fig. 7 shows changes in the intracellular GSH level in CR cells treated with cisplatin and NCX-4016. Whereas cells treated with cisplatin did not show any significant change in their thiol content, cells treated with 100 μM NCX-4016 showed a substantially reduced level of GSH (50.3 ± 8.1%). Secondary incubation of the NCX-4016-treated cells with cisplatin did not show any significant change in the GSH level compared with the cells treated with NCX-4016 alone. The data suggested that GSH was involved in the antiproliferative action of NCX-4016 in CR cells.

Discussion

NCX-4016 belongs to a new class of nonsteroidal antiinflammatory drugs (NSAIDs) capable of releasing NO. Unlike conventional NO donors that release NO in aqueous solutions, NCX-4016 releases NO only after intracellular enzymatic conversion (11, 13). The drug has been shown to release sustained amounts of NO *in vivo* (14, 15). Although the use of NSAIDs is limited by their gastrointestinal (GI) and renal toxicity, NO-releasing NSAIDs were shown to exert antiinflammatory and analgesic effects that were at least as potent as those of the parent drug, without causing GI tract toxicity (16–19). The *in vivo* metabolism of these drugs has been established reasonably well in a rat model (14, 20), except that the precise mechanism by which NO is released from the nitro moiety has yet to be understood. NCX-4016 is metabolized by esterases in the liver cells and in plasma to salicylic acid and 3-(nitrooxymethyl)phenol, which is rapidly metabolized to 3-hydroxybenzylalcohol and NO (20). The carbon atom of 3-(nitrooxymethyl)phenol can react with GSH to form 1-(glutathion-*S*-yl)methylene-3-hydroxybenzene. This process is enzymatically mediated by GSH transferase and is dependent on the availability of GSH (20). Napoli *et al.* (21, 22) showed that NCX-4016 reduced experimental restenosis, an effect associated with lower vascular smooth muscle cell proliferation. The slow and sustained release of NO seems to be the reason for its nontoxic nature, safe profile, and ability to intervene with the pathological process.

The EPR spectroscopy analysis offered direct evidence that NO was generated from NCX-4016 in the CR cells upon treatment with the drug. The absence of an NO adduct signal in cells not treated with NCX-4016 indicated the participation of certain cellular enzyme(s) in the metabolic conversion of NCX-4016. NO was released slowly and continued beyond 90 min of treatment. This is in sharp contrast to many other NO donors that release NO over a short duration (<10 min) and without requiring any enzymatic conversion. The *in vivo* and *in vitro* metabolism of NCX-4016 has been recently investigated in rat venous blood by using EPR spectroscopy (14). It was shown that NCX-4016 undergoes rapid metabolism, with the formation of salicylic acid and a nitro moiety, wherein the latter is metabolized to release NO via some unknown mechanism. NO-Fe(II)-Hb, formed by NO reaction with heme proteins, was detectable in the venous blood 1 h after dosing, and its formation was maximal at 4–6 h after dosing (10, 14). However, the exact mechanism and kinetics of the metabolic conversion of NCX-4016 in the cellular environment are not known at present.

The antiproliferative effects of cisplatin on the two currently studied cell lines were clearly different. The markedly higher IC_{50} value of cisplatin in exerting cytotoxicity in CR cells compared with that in CS cells is characteristic of cisplatin resistance. The refractory nature of the CR cells was further confirmed by the higher levels of cellular GSH (Fig. 7). The levels of GSH in the resistant cells were 75 ± 10% higher than those in the sensitive cells. Thus, these observations confirmed that the two cell lines were, in fact, characterized as CS and CR.

The present results clearly demonstrated that NCX-4016, by itself, was cytotoxic to HOCCs. The cytotoxicity of NCX-4016 in CR cells was also comparable with that in the CS cells (Fig. 4), suggesting that NCX-4016 was not subject to the thiol resistance that was observed with cisplatin. The antiproliferative nature of NCX-4016 could be attributed to its ability to generate sustained amounts of NO in the cells. This was further confirmed by the observations that short-term (1 h) treatment of CR cells with NCX-4016 or with SIN-1 failed to induce any significant antiproliferative effect. Furthermore, the fact that cytotoxicity was only observed with NCX-4016 but not with aspirin [acetylsalycylic acid (ASA)] suggested that aspirin failed to contribute to the observed cell killing by the drug.

A recent study reported that NCX-4016 and a few other related NO NSAIDs exerted remarkable cytotoxicity in human cancer cell lines of adenomatous and squamous origins with a wide variety of tissue targets (13). NCX-4016, in particular, was consistently the most potent cytotoxic agent in all cell lines studied, and its effect, unlike that of aspirin, was cyclooxygenase-independent.

In general, it was observed that NCX-4016 was more effective than cisplatin in inducing the cytotoxic effect. This was evident from the current study with CR, CS, and CHO cells (Fig. 6). The efficacy and dose-dependent effect of NCX-4016 in the cancer cells revealed that cellular GSH had no effect on the action of the drug, because a similar extent of cytotoxicity was observed in the two cell lines. It was apparent that NCX-4016 was capable of overcoming the thiol-mediated cytoprotection in CR cells. The thiol data from CR cells suggested that an ≈50% reduction in GSH levels was achieved upon treatment with NCX-4016 (Fig. 7). The thiol depletion could cause cells to bypass their refractory nature and could sensitize them to further treatment with cisplatin. This was achieved by pretreating CR cells with NCX-4016 for 6 h and then treating them with cisplatin for 1 h. The results indicated that substantially enhanced cell killing was obtained by pretreating CR cells with NCX-4016 (Fig. 6). Assuming that NCX-4016 caused a 30% killing of CR cells (Fig. 6) and that cisplatin could cause a 32% cell killing of CS cells, which was presumably similar to the NCX-4016-pretreated

(thiol-depleted) CR cells, we estimated the effective cell killing to be 52%. This corresponded to a survival of 48%, which agreed closely with the observed survival of 48% in the combined treatment with NCX-4016 and cisplatin of CR cells. Overall, the results suggested a dual role for NCX-4016 in CR cells: antiproliferative effect and thiol depletion. The thiol depletion creates an opportunity for cisplatin for further cell killing. This observation has important implications in the development of treatment modalities for ovarian cancer.

There are, however, still several questions that remain to be answered. The involvement of GSH in the bioactivation/bioconversion and antiproliferative action of NCX-4016 in HOCCs has not been clearly established by the present study. The mechanism of the cytotoxic effect of NCX-4016 may be entirely different from that of cisplatin. However, the present results from cells in culture will be useful in studies with animals, *in vivo*.

In summary, NCX-4016, a nitroaspirin, belongs to a new class of NSAIDs. NCX-4016 releases sustained amounts of NO in cells and *in vivo*. We investigated the cytotoxic effect of this drug in two HOCC lines: CS cells, which responded to cisplatin treatment, and CR cells, which were refractory to cisplatin treatment apparently because of higher levels of intracellular thiols. The cells were treated with NCX-4016 and/or cisplatin and assayed for clonogenecity. EPR spectroscopy was used to confirm the release of NO in cells treated with NCX-4016. The data showed that treatment of the cancer cells with NCX-4016 for 6 h resulted in a significant reduction in the colony-forming ability of the cells. The CR cells subjected to NCX-4016 treatment showed a more pronounced reduction in the surviving fraction and cellular GSH levels, compared with those subjected to cisplatin treatment. CR cells pretreated with NCX-4016 and then treated with cisplatin showed significantly greater toxicity when compared with those treated with NCX-4016 or cisplatin alone. The thiol-depleting ability of NCX-4016 caused these cells to regain cisplatin sensitivity. Thus, NCX-4016 was a potent inhibitor of the proliferation of CR ovarian cancer cells as well as a sensitizer of CR cells for treatment with cisplatin in patients with recurrent ovarian cancer.

Materials and Methods

Reagents. Nitroaspirin [2-(acetyloxy)benzoic acid 3-(nitrooxymethyl)phenyl ester; NCX-4016] was obtained from NicOx (Sophia Antipolis, France). GSH (L-glutamyl-L-cysteinylglycine), aspirin, DMSO, SIN-1 hydrochloride, SNAP, trypan blue, and crystal violet were obtained from Sigma. Cisplatin [*cis*-diamminedichloroplatinum(II)], ammonium iron(II) sulfate hexahydrate, and acetonitrile were purchased from Aldrich. Cell culture medium (RPMI medium 1640), FBS, antibiotics, sodium pyruvate, trypsin, and PBS were purchased from GIBCO/BRL. The imidazoline biradical probe, used for thiol measurements, was a gift from Valery Khramtsov (Russian Academy of Science, Novosibirsk, Russia). MGD was synthesized and purified in our laboratory (23).

Cells. CR and CS HOCCs were obtained from Raj Sridhar (Howard University Medical School, Washington, DC). Cells were grown in RPMI medium 1640 supplemented with 10% FBS, 2% sodium pyruvate, and 1% penicillin/streptomycin. Cells were plated at a density of 5×10^4 and 1.2×10^6 in 60- and 100-mm dishes for drug treatment (NCX-4016 and cisplatin) and determination of GSH, respectively. Cells were grown up to 70% confluence in 75-cm^2 flasks for determination of intracellular NO release. Culture and drug treatment(s) of cells were carried out at 37°C in an atmosphere of 5% CO_2 and 95% air. Cells were routinely trypsinized (0.05% trypsin/EDTA) and counted by using a hemacytometer. Cell viability was determined by the trypan blue dye exclusion method.

Cell-Survival Assay. Cell survival was assessed by clonogenic assay. Cells at ≈80% confluence were trypsinized, rinsed, seeded onto 60-mm dishes (5×10^4 cells per dish), grown for 24 h at 37°C, and treated afterward with cisplatin, NCX-4016, SIN-1, or aspirin for 1 or 6 h. After treatments, cells were washed twice with PBS, trypsinized, counted, and plated in 60-mm dishes in triplicate and incubated for 7 days. On day 7, the colonies were stained with crystal violet (in ethyl alcohol) and counted. Each experiment was repeated at least five times.

Cell colonies were counted by using a ColCount automated colony counter (Oxford Optronix, Oxford, U.K.). ColCount was designed to accurately reproduce the proportionality of manual counting methods and to yield highly comparable results of the surviving fraction and, hence, similar survival curves. It uses a high-resolution charge-coupled device camera to capture the image of stained cells in the entire dish. The image is then analyzed to identify (contour) the colonies and to perform a quantitative analysis. The technique provides detailed information on the radius, area, density, and distance to nearest neighbor of the colonies. Postprocessing options permit a variety of user-selectable parameters that can be used to set inclusion/rejection criteria. Colonies in the range of 0.1–1 mm were scored in all experiments.

GSH Assay. Cellular levels of GSH were determined by EPR spectroscopy, which was based on the application of an imidazoline biradical label (24). The label reacts with reduced thiol and shows a characteristic EPR spectrum, which can be quantified by using known amounts of GSH. Cells (2.5×10^6 cells per milliliter) were trypsinized, counted, and treated with the thiol-specific label (0.5 mM) at pH 7.0 for 7 min, after which their EPR spectra were measured. The concentration of GSH was determined from a standard curve prepared with known concentrations of GSH under similar conditions.

EPR Spectroscopy Measurements. CR and CS HOCCs grown to 70% confluence in 75-cm^2 flasks were trypsinized, and cell suspensions at 2×10^7 cells per milliliter were prepared and then treated with 500 μM NCX-4016 for the desired lengths of time. Cell suspensions were incubated at room temperature. The NO spin trap $(MGD)_2Fe(II)$ was prepared by mixing 1 mM Fe^{2+} [ammonium iron(II) sulfate hexahydrate] with 5 mM MGD and then was added to the cell suspension. The measurements were performed by using an X-band EPR spectrometer. The EPR spectra were measured by using 20-mW microwave power, 3-G modulation amplitude (1 G = 0.1 mT), 100-kHz modulation frequency, 16-msec time constant, 100-G scan range, and 30-sec scan time. SNAP was used as an authentic positive control for NO trapping.

Statistical Analysis. Data were expressed as mean ± SEM. Comparisons among groups were performed by using Student's *t* test. The significance level was set at $P < 0.05$.

This work was supported by National Institutes of Health Grants RR003048, CA78886, and CA102264.

1. Greenlee, R. T., Hill-Harmon, M. B., Murray, T. & Thun, M. (2001) *CA Cancer J. Clin.* **51,** 15–36.
2. Harries, M. & Gore, M. (2002) *Lancet Oncol.* **3,** 529–545.
3. Johnson, S. W., Ozols, R. F. & Hamilton, T. C. (1993) *Cancer* **71,** 644–649.
4. Piccart, M. J., Lamb, H. & Vermorken, J. B. (2001) *Ann. Oncol.* **12,** 1195–1203.
5. Ignarro, L. J., Buga, G. M., Wei, L. H., Bauer, P. M., Wu, G. & del Soldato, P. (2001) *Proc. Natl. Acad. Sci. USA* **98,** 4202–4208.
6. Ongini, E., Impagnatiello, F., Bonazzi, A., Guzzetta, M., Govoni, M., Monopoli, A., Del Soldato, P. & Ignarro, L. J. (2004) *Proc. Natl. Acad. Sci. USA* **101,** 8497–8502.

7. Wink, D. A., Cook, J. A., Christodoulou, D., Krishna, M. C., Pacelli, R., Kim, S., DeGraff, W., Gamson, J., Vodovotz, Y., Russo, A. & Mitchell, J. B. (1997) *Nitric Oxide* **1,** 88–94.
8. Riganti, C., Miraglia, E., Viarisio, D., Costamagna, C., Pescarmona, G., Ghigo, D. & Bosia, A. (2005) *Cancer Res.* **65,** 516–525.
9. Birnboim, H. C. & Privora, H. (2000) *Nitric Oxide* **4,** 496–504.
10. Chen, Z., Zhang, J. & Stamler, J. S. (2002) *Proc. Natl. Acad. Sci. USA* **99,** 8306–8311.
11. Wallace, J. L., Ignarro, L. J. & Fiorucci, S. (2002) *Nat. Rev. Drug Discov.* **1,** 375–382.
12. Feelisch, M., Schonafinger, K. & Noack, E. (1992) *Biochem. Pharmacol.* **44,** 1149–1157.
13. Kashfi, K., Ryann, Y., Qiao, L. L., Williams, J. L., Chen, J., Del Soldato, P., Traganos, F. & Rigas, B. (2002) *J. Pharmacol. Exp. Ther.* **303,** 1273–1282.
14. Carini, M., Aldini, G., Stefani, R., Orioli, M. & Facino, R. M. (2001) *J. Pharm. Biomed. Anal.* **26,** 509–518.
15. Muscara, M. N., Lovren, F., McKnight, W., Dicay, M., del Soldato, P., Triggle, C. R. & Wallace, J. L. (2001) *Br. J. Pharmacol.* **133,** 1314–1322.
16. Fiorucci, S., Santucci, L., Cirino, G., Mencarelli, A., Familiari, L., Soldato, P. D. & Morelli, A. (2000) *J. Immunol.* **165,** 5245–5254.
17. Fiorucci, S., Mencarelli, A., Meneguzzi, A., Lechi, A., Morelli, A., del Soldato, P. & Minuz, P. (2002) *Circulation* **106,** 3120312–3120315.
18. Bak, A. W., McKnight, W., Li, P., Del Soldato, P., Calignano, A., Cirino, G. & Wallace, J. L. (1998) *Life Sci.* **62,** 367–373.
19. al-Swayeh, O. A., Clifford, R. H., del Soldato, P. & Moore, P. K. (2000) *Br. J. Pharmacol.* **129,** 343–350.
20. Carini, M., Aldini, G., Orioli, M. & Maffei Facino, R. (2002) *J. Pharm. Biomed. Anal.* **29,** 1061–1071.
21. Napoli, C., Cirino, G., Del Soldato, P., Sorrentino, R., Sica, V., Condorelli, M., Pinto, A. & Ignarro, L. J. (2001) *Proc. Natl. Acad. Sci. USA* **98,** 2860–2864.
22. Napoli, C., Aldini, G., Wallace, J. L., de Nigris, F., Maffei, R., Abete, P., Bonaduce, D., Condorelli, G., Rengo, F., Sica, V., *et al.* (2002) *Proc. Natl. Acad. Sci. USA* **99,** 1689–1694.
23. Kuppusamy, P., Wang, P., Samouilov, A. & Zweier, J. L. (1996) *Magn. Reson. Med.* **36,** 212–218.
24. Khramtsov, V. V., Yelinova, V. I., Weiner, L. M., Berezina, T. A., Martin, V. V. & Volodarsky, L. B. (1989) *Anal. Biochem.* **182,** 58–63.

BIOGRAPHICAL SKETCH

Provide the following information for the key personnel in the order listed on Form Page 2.
Follow this format for each person. **DO NOT EXCEED FOUR PAGES.**

NAME	POSITION TITLE
Xing-Jie Liang, Ph.D.	Assistant Professor

EDUCATION/TRAINING *(Begin with baccalaureate or other initial professional education, such as nursing, and include postdoctoral training.)*

INSTITUTION AND LOCATION	DEGREE *(if applicable)*	YEAR(s)	FIELD OF STUDY
Hebei Normal University, China	B.S.	July 1993	Biochemistry
College of Life Science, NanKai University, China	M.S.	July 1997	Genetics and Engineering of Microbiology
Institute of Biophysics, Chinese Academy of Science, China	Ph.D.	July 2000	Biophysics, Biochemistry and Molecular Biology

Employment:

1994 - 1997 Research Assistant, College of Life Science, NanKai University, China
1997 - 2000 Research Associate, Institute of Biophysics, Chinese Academy of Sciences, China
2000 - 2005 Postdoc, NCI, NIH, USA
2005 - 2007 Research Fellow, Surgical Neurology Branch, NINDS,NIH, USA
2007 - Assistant Professor, Department of Radiology, Howard University, Washington, DC

Honors, Grants and Prizes

1. Invited speaker for “International ABC Genes and Diseases Workshop”, Oct 21, NCI-Frederick, 2004
2. "Fellows Award for Research Excellence" National Institute of Health, Bethesda, USA, 2006.
3. Fogarty International Fellowship, National Institute of Health, 2000-2005.
4. "Fellows Award for Research Excellence" National Institute of Health, Bethesda, USA, 2005.
5. “Chair’s award” for Gordon Research Conference on “drug carriers in medicine and biology”, Big Sky, Montana, 2004.
6. "Fellows Award for Research Excellence" National Institute of Health, Bethesda, USA, 2004.
7. "Young Scientist Fellowship" for 18th International Congress of Biochemistry and Molecular Biology, Birmingham, England, 2000.
8. "DiAo Award" for excellent research paper, Chinese Academy of Science, China, 2000.
9. “Excellent Research Award” for group of oil microbiology in Nankai University, China, 1999.
10. "Guang Hua Scholarship" for graduate students in NanKai University, China, 1997.
11. “Excellent Student” for undergraduate in HeBei Normal University, 1993.

Gene cloned in Genbank: Xing-Jie Liang and Michael M. Gottesman, γ-catenin nucleotide sequence, GenBank accession number: AY243535. Feb, 2003.

Memberships

1. American Association for Cancer Research (Since 2001)
2. American Society for Cell Biology (Since 2002)
3. Association of the International Union against Cancer (Since 2003)
4. Member of NCI, CCR fellows’ editorial board (Since 2003)
5. Vice President, Chinese Scholars' Association at NIH (Since 2005)

6. Tutor of NIH National Graduate Students Research Festival (2006)

Publications

1. Liang, X. J. and Aszalos A. Multidrug transporters as drug targets. Current Drug Targets, 2006, 7 (8): Aug 911-921.
2. Liang, X. J., Mukherjee, S., Shen, D. W., Maxfield, F. R. and Gottesman, M. M. Endocytic Recycling Compartments Altered in Cisplatin-Resistant Cancer Cells . Cancer Research, 2006, 66 (4): Feb 15; 2346-2353.
3. Shen, D.W., Liang, X. J., Suzuki, T., and Gottesman, M. M. Identification by Functional Cloning From a Retroviral cDNA Library of cDNAs for Ribosomal Protein L36 and Heat Shock Protein 10 That Confer Cisplatin Resistance. Molecular Pharmacology, 2006, 69(4): Jan 4; 1383-1388.
4. Liang, X. J., Taylor B, Cardelli C, Yin JJ, Annereau JP, Garfield SH, Wincovitch S, Szakacs G, Gottesman, M. M and Aszalos A. Different roles for K+ channels in cisplatin resistant cell lines Argue Against a Critical Role for These Channels in Cisplatin Resistance. Anticancer Research, 2005, 25(6B): 4113-4122.
5. Liang, X. J., Shen, D. W., Chen G. K., Wincovitch S. M., Garfield, S., and Gottesman, M. M. Trafficking and localization of platinum complexes in cisplatin-resistant cell lines monitored by fluorescence-labeled platinum. Journal of Cellular Physiology, 2005, 202 (3): 635-641.
6. Kevin G. Chen, Gergely Szakacs, Jean-Philippe Annereau, Francois Rouzaud, Xing-Jie Liang, Julio C. Valencia, Chandrasekharam N. Nagineni, John J. Hooks, Vincent J. Hearing, and Michael M. Gottesman. Principal Expression of the Two mRNA Isoforms (ABCB5α and ABCB5β) of the ATP-Binding Cassette Transporter ABCB5, In Melanoma Cells and In Melanocytes. Pigment Cell Research, 2005, 18 (2): 102-112.
7. Liang, X.J, Shen, D.W, and Gottesman, M.M. Down-regulation and altered localization of γ-catenin in cisplatin-resistant adenocarcinoma cells. Molecular Pharmacology, 2004 65 (5): 1217-1224.
8. Liang, X.J, Shen, D.W, and Gottesman, M.M. A pleiotropic defect reducing drug accumulation in cisplatin-resistant cells. Journal of Inorganic Biochemistry, 2004 (98) 1599-1606.
9. Shen, D.W, Liang, X.J, and Gottesman, M.M. Identification of cytoskeletal [14C] carboplatin-binding proteins reveals reduced expression and disorganization of actin and filamin in cisplatin-resistant cell lines. Molecular Pharmacology, 2004, 66(4): 789-793.
10. Liang, X.J, Yin, J.J., Zhou, J.W., Wang, P. C., Taylor, B., Cardarelli, C., Kozar, M, Forte, R., Aszalos, A. and Gottesman, M. M.: Changes in biophysical parameters of plasma membranes influence cisplatin resistance of sensitive and resistant epidermal carcinoma cells. Experimental Cell Research, 293: 283-291, 2004.
11. Shen, DW, Su, A, Liang, X.J, Pai-Panandiker, A, and Gottesman, MM. Reduced expression of small GTPases and hypermethylation of the folate binding protein gene in cisplatin-resistant cells. British Journal of Cancer, 91(2): 270-276, 2004.
12. Liang, X. J., Shen, D. W., Garfield, S., and Gottesman, M. M. Mislocalization of membrane proteins associated with multidrug resistance in cisplatin-resistanct cancer cell lines. Cancer Research, 63: 5909-5916, 2003.
13. Aleman, CS., Annereau, J.P., Liang, X.J., Carderelli, C., Taylor, B., Yin, J.J., Aszalos, A., and Gottesman, M.M. P-glycoprotein effects on biophysical membrane properties using an inducible system. Cancer Research, 63: 3084-3091, 2003.
14. Chauhan, S. S, Liang, X.J, Su, A.W, Pai-Panandiker, A, Shen, D.W., Hanover, J.A., and Gottesman, MM. Reduced endocytosis and altered lysosome function in cisplatin resistant cell lines. British Journal of Cancer, 88: 1327-1334, 2003.
15. Ying, Y. M., Shen, D. W., Liang, X. J., and Gottesman, M. M. Codominance of Cisplatin Resistance in Somatic Cell Hybrids. Journal of Cellular Physiology, 196: 63-69, 2003.
16. Liang, X. J. and Huang, Y. G. Physical state changes of membrane lipids in human lung adenocarcinoma A549 cells and its resistance to cisplatin. The International Journal of Biochemistry and Cell Biology. 34: 1248-1255, 2002.
17. Liang, X. J. and Huang, Y. G.: Phospholipid flippase associates with cisplatin resistance in plasma membrane of lung adenocarcinoma A549 cells. Prog. Nat. Sci. 11: 226-230, 2001.

18. Liang, X. J. and Huang, Y. G.: Alteration of membrane lipid biophysical properties and resistance of human lung adenocarcinoma A549 cells to cisplatin. Science in China. 44: 25-32, 2001.
19. Diao, H.X., Liang, F.L., Liang, X.J., Yang, S.J., Liu, R.L. Studies on the synergism of interaction of Xanthan NK-01 and galactomannan. Acta Scientiarum Naturalium Universitatis Nankaiensis . 34 (1): 15-20, 2001.
20. Liang, X.J. Study on the effect of membrane lipids and intracellular signals on cisplatin resistance in the human multidrug resistance lung adenocarcinoma A549 cells. Dissertation for Doctor of Philosophy, 2000.
21. Liang, X. J. and Huang Y. G.: Intracellular free calcium concentration and cisplatin resistance in human lung adenocarcinoma A549 cells. Bioscience Reports, 20: 129-138, 2000.
22. Liang, X. J. and Huang, Y. G.: Cisplatin resistance in lung carcinoma cancer cells with flippase on the plasma membrane. Progress in Natural Science 11: 194-198, 2001.
23. Liang, X. J. and Huang, Y. G.: Plasma membrane state changement affects the cisplatin resistance in the lung carcinoma cancer cells. Science in China (C), 30: 607-613, 2000.
24. Liang, X. J., Huang, Z. H., Lu, Y. M., Li, Y. M., and Huang, Y. G.: Change of cell cycle and resistance of A549 cells to cisplatin. Prog. Biochem. Biophys. 27: 616-620, 2000.
25. Liang, X.J. Study on the carrier lipid in membrane and Xanthan gum of Xanthamonas Campestris NK-01. Thesis for Master of Science, 1997.

Submitted Manuscript

26. Liang, X. J., Shen, D.W., Yin, J.J., Aszalos, A., and Gottesman, M. M. SIRT1 Plays an Essential Role in Tumor Resistance to Cisplatin by Restricting Glucose Metabolism. (EMBO J, submitted for review).
27. Ngo.T.B*, Peng T., *, Liang X.J *., Akeju O., Pastorino S., Zhang W., Fine H.A., Maric D., Wen P.Y., Girolami U.D., Black P.M., Wu W., Shen R.F., Kang D.W., and Park J.K. The 1p encoded protein stathmin modulates the response of malignant gliomas to nitrosoureas (Journal of Clinical Investigation, in Review) [*: Equal contribution]
28. Liang, X.J. and Park, J.K. Inhibition of stathmin enhances CCNU blocking glioma cell migration and invasion. (Preparing for Cancer Research).